ANANSE: An enhancer network-based computational approach for predicting key transcription factors in cell fate determination

Quan Xu[1], Georgios Georgiou[1,2], Gert Jan C. Veenstra[1], Huiqing Zhou[1,3,*] and Simon J. van Heeringen[1,*]

[1] Department of Molecular Developmental Biology, Faculty of Science, Radboud Institute for Molecular Life Sciences, Radboud University, 6525GA Nijmegen, The Netherlands.

[2] Current address: Viroclinics Biosciences BV, Rotterdam 3029 AK, The Netherlands.

[3] Department of Human Genetics, Radboud Institute for Molecular Life Sciences, Radboud University Medical Center, 6525GA Nijmegen, The Netherlands.

[*] Correspondence: s.vanheeringen@science.ru.nl; j.zhou@science.ru.nl; Tel +31-24-3616850

Abstract

Proper cell fate determination is largely orchestrated by complex gene regulatory networks centered around transcription factors. However, experimental elucidation of key transcription factors that drive cellular identity is currently often intractable. Here, we present ANANSE (ANalysis Algorithm for Networks Specified by Enhancers), a network-based method that exploits enhancer-encoded regulatory information to identify the key transcription factors in cell fate determination. As cell type-specific transcription factors predominantly bind to enhancers, we use regulatory networks based on enhancer properties to prioritize transcription factors. First, we predict genome-wide binding profiles of transcription factors in various cell types using enhancer activity and transcription factor binding motifs. Subsequently, applying these inferred binding profiles, we construct cell type-specific gene regulatory networks, and then predict key transcription factors controlling cell fate conversions using differential gene networks between cell types. This method outperforms existing approaches in correctly predicting major transcription factors previously identified to be sufficient for trans-differentiation. Finally, we apply ANANSE to define an atlas of key transcription factors in 18 normal human tissues. In conclusion, we present a ready-to-implement computational tool for efficient prediction of transcription factors in cell fate determination and to study transcription factor-mediated regulatory mechanisms. ANANSE is freely available at https://github.com/vanheeringen-lab/ANANSE.

Keywords: Enhancer, Transcription Factor, Gene Regulatory Network, Cell Fate Determination

Introduction

Every multicellular organism develops from a single cell. During this process, cells undergo division and differentiation, eventually forming a diversity of cell types that are organized into organs and tissues. How one cell develops into different cell types, a process known as cell fate determination, is critical during development. It has been shown that transcription factors (TFs) play key roles in cell fate determination (Davis et al., 1987; Jopling et al., 2011; Pang et al., 2011; Stadhouders et al., 2019; Takahashi et al., 2007; Vierbuchen et al., 2010). TFs bind to specific cis-regulatory sequences in the genome, including enhancers and promoters, and regulate expression of their target genes (Lambert et al., 2018; Vaquerizas et al., 2009). The interactions between TFs and their downstream target genes form gene regulatory networks (GRNs), controlling a dynamic cascade of cellular information processing (Davidson, 2010; Tegner and Bjorkegren, 2007). Cell fate determination is orchestrated by a series of TF regulatory events, largely by complex GRNs (Wilkinson et al., 2017). The key role of TFs and GRNs in cell fate determination is further corroborated by examples of cell fate conversions, often referred as cellular reprogramming (Iwafuchi-Doi and Zaret, 2016; Peñalosa-Ruiz et al., 2019). Cellular reprogramming includes generating induced pluripotent stem cells (iPSCs) from somatic cells, and trans-differentiation that converts one mature somatic cell type to another without undergoing an intermediate pluripotent state (Davis et al., 1987; Jopling et al., 2011; Pang et al., 2011; Stadhouders et al., 2019; Takahashi et al., 2007; Vierbuchen et al., 2010). These reprogramming processes are initiated by enforced expression of combinations of different key TFs, which is believed to alter the output of GRNs in the cell, namely gene expression and the epigenetic landscape (Buschbeck and Hake, 2017; Qu et al., 2018; Reik et al., 2001).

In the past, identification of key TFs driving cellular differentiation or reprogramming were often performed with experimental screening or testing individual genes, which is labor-intensive and inefficient. Therefore, there is a need for better predictions of key TFs in cell fate determination that can help to understand developmental processes or serve to instruct experimental cellular reprogramming approaches. Several computational methods for predicting key transcription regulators, such as TFs in the context of cell fate conversion, have been reported. Many methods only consider GRNs based on gene expression levels and differences in gene expression

between cell types, and identify candidate key TFs with high expression in the target cell types (Cahan et al., 2014; D'Alessio et al., 2015; Hartmann et al., 2018; Heinaniemi et al., 2013; Lang et al., 2014; Morris et al., 2014; Roost et al., 2015). Mogrify uses not only gene expression but also GRNs constructed based on TF binding motifs in promoters to predict TFs that are capable of inducing conversions between cell types (Rackham et al., 2016). Although these methods can perform reasonably well and prioritize a short list of predicted key TFs for some cell fate conversions, e.g. SOX2 during fibroblasts to iPSCs, the current computational tools do not take enhancers into consideration. It has been well established that TFs that control tissue- and cell type-specific gene expression in cell fate determination and development often bind to enhancers (Andersson et al., 2014; Bulger and Groudine, 2011; Qu et al., 2018; Spitz and Furlong, 2012). Binding of tissue- and cell type-specific TFs largely to enhancers is also confirmed by a large number of genome-wide chromatin immunoprecipitation followed by sequencing analyses (ChIP-seq) (Davis et al., 2018; Valouev et al., 2008), e.g. TP63 in keratinocytes and ZIC2 in embryonic stem cells (Luo et al., 2015; Qu et al., 2018). Therefore, a computational method that uses enhancer properties and enhancer-based GRNs may improve the prediction of key transcriptional regulators. Furthermore, most current computational tools require comprehensive training or background data, such as cell/tissue expression data or pre-constructed networks. This means that they cannot be applied in new biological contexts or in species that are less well-studied. Finally, these datasets and the computational algorithms are not always publicly accessible, which prevents the general usage of these methods in studying transcriptional regulation or designing new trans-differentiation strategies.

In this study, we established an enhancer GRN-based method, ANalysis Algorithm for Networks Specified by Enhancers (ANANSE), that infers genome-wide regulatory programs and identifies key TFs for cell fate determination. First, we systematically analyzed the peaks of all publicly available human TF ChIP-seq experiments as processed by the ReMap project (Chèneby et al., 2017), confirming that most cell type- and tissue-specific TFs predominantly bind to enhancers. We then predicted cell type-specific TF binding profiles with a model based on activities and sequence features of enhancers. Second, combining TF binding profiles and gene expression data, we built cell type-specific enhancer GRNs in each cell type or tissue. We used reference GRNs based on gene expression, Gene Ontology terms and TF-target gene interactions to evaluate the quality of our inferred networks. Third, we predicted the key TFs underlying cell fate conversions based on a differential network analysis. Compared with other reported prediction algorithms, ANANSE recovers the largest fraction of TFs that were validated by experimental trans-differentiation approaches. The results demonstrate that ANANSE accurately prioritizes TFs that drive cellular fate changes. Finally, to demonstrate the wide utility of ANANSE, we applied it to 18 human tissues and generated an atlas of key TFs underlying human tissue identity.

Materials and Methods

Datasets

The 296 ChIP-seq datasets for the peak location analysis were downloaded from ReMap 2018 (Chèneby et al., 2017). For training and evaluation of the regression model to predict TF binding TF ChIP-seq data from 5 different cell lines (GM12878, hESC, HeLa-S3, HepG2 and K562) was downloaded from the ENCODE-DREAM project (https://www.synapse.org/ENCODE) (ENCODE-DREAM, 2017). The H3K27ac ChIP-seq data of training cell lines and validation cell lines (GM12878 (ENCFF948GTC), hESC (ENCFF238SQN), HeLa-S3 (ENCFF218BUW), HepG2 (ENCFF686HFQ), K562 (ENCFF301TVL), Liver (ENCFF435RWI), MCF-7 (ENCFF692SZU), and PC-3 (ENCFF474QFK)) was downloaded from the ENCODE project (ENCODE Project Consortium, 2012). The non-redundant database of 1,690 motifs for 1,164 TFs was created by clustering all vertebrate motifs from the CIS-BP database using GimmeMotifs (van Heeringen and Veenstra, 2010; Weirauch et al., 2014) as described in (Bruse and Heeringen, 2018).

The RNA-seq data used to predict key TFs for trans-differentiation was obtained from the following accessions: Astrocyte (GSE104232) (Tchieu et al., 2019), Cardiomyocyte (GSE88167) (ENCODE Project Consortium, 2012), Fibroblast (GSE120131) (van der Raadt et al., 2019), Hepatocyte (PRJNA239637) (ENCODE Project Consortium, 2012), iPSC (GSE120107) (Soares et al., 2019), Keratinocyte (GSE78592) (ENCODE Project Consortium, 2012), Macrophage (GSE85243) (Novakovic et al., 2016), Osteocyte (GSE78608) (ENCODE Project Consortium, 2012). All the H3K27ac ChIP-seq data used to predict key TFs for trans-differentiation was downloaded from ENCODE project: Astrocyte (GSM733763), Cardiomyocyte (GSM2527377), Fibroblast (GSM733662), Hepatocyte (GSM2534083), iPSC (GSM706065), Keratinocyte (SRR2172653), Macrophage (GSM2262949), and Osteocyte (GSM733739) (ENCODE Project Consortium, 2012).

ChIP-seq and RNA-seq analyses

The reads of the ChIP-seq experiments were mapped to the human genome (hg38) using STAR (version 2.5.3a) with default settings (Dobin et al., 2013). Duplicate reads were marked and removed using Picard (Picard2019toolkit, 2019). Peaks were called on the ChIP-seq data with only the uniquely mapped reads using MACS2 (version 2.7) relative to the Input track using the standard settings and a q-value of 0.01 (Zhang et al., 2008). The measurement of consistent peaks between replicates was identified by IDR (version 2.0.3) (Li et al., 2011). Quantification of expression levels was performed on RNA-seq data, using salmon (version 0.43.0) (Patro et al., 2017) with default settings and Ensembl transcript sequences (version GRCh38 release-94) (Cunningham et al., 2018). Salmon's transcript-level quantifications results were imported and aggregated to gene level counts by the tximport R package (version 1.12.3) (Soneson et al., 2015). The expression level (transcript-per-million, TPM) of each cell type and the differential expression fold change between two cell types were calculated using the DESeq2 R package (version 1.24.0) (Love et al., 2014). The expression TPM data used to predict key TFs for trans-differentiation is shown in Supplementary Table S1, differential gene expression data is shown in Supplementary Table S2, and the enhancer data is shown in Supplementary Table S3.

Analysis of the genomic distribution of TF binding sites

For every TF, we combined all the peaks in the ReMap database (Chèneby et al., 2017) by taking the peaks in all cell types and tissues for this specific TF. TFs that had less than 600 peaks were removed. The percentage of peaks in each genomic location was calculated using the ChIPseeker R package (version 1.20.0) (Yu et al., 2015). The fgsea R package (version 1.10.1) was used to do the gene set enrichment analysis (GSEA) (Sergushichev, 2016).

Defining putative enhancer regions

To generate a collection of putative enhancer regions, we collected all transcription factor ChIP-seq peaks from ReMap 2018 (http://remap.univ-

amu.fr/storage/remap2018/hg38/MACS/remap2018_all_macs2_hg38_v1_2.bed.gz) (Chèneby et al., 2017). We took the summit of all peaks and extended these 25 bp up- and downstream. Based on this file, we generated a coverage bedGraph using bedtools genomecov (Quinlan and Hall, 2010). We performed peak calling on this bedGraph file using bdgpeakcall from MACS2 (version v2.7.1) (Zhang et al., 2008), with the following settings: l=50 and g=10. We performed the peak calling twice, setting c to 4 and 30, respectively. All peaks from c=30 were combined with all peaks of c=4 that did not overlap with the peaks of c=30. We then removed all regions on chrM and extended the summit of the peaks 100 bp up- and downstream to generate a final collection of 1,268,775 putative enhancers of 200 bp. This collection of enhancers is available at Zenodo with doi 10.5281/zenodo.4066423.

The multiBamCov tool (version v2.29.2) (Quinlan and Hall, 2010) was used to determine the H3K27ac intensity, as expressed by the number of reads, in all enhancer peaks (2,000 bp centered at the enhancer summit). Quantile normalization was applied to all enhancers to let the enhancer data of samples have the same distribution with training data. The enhancers that overlapped with H3K27ac ChIP-seq broadPeaks were selected as final enhancers of individual cell type.

Prediction of transcription factor binding

Binding was predicted using a standard logistic regression model (Eq. 1) as implemented in scikit-learn (Pedregosa et al., 2011).

$$\log\frac{p_{f,l}}{1-p_{f,l}} = \beta_1 S_{f,l} + \beta_2 E_l \qquad (1)$$

Where $p_{f,l}$ is the probability of a transcription factor f binding to enhancer l. $S_{f,l}$ is the highest motif z-score of all motifs associated with transcription factor f in enhancer l and E_l is the scaled enhancer intensity of enhancer l.

The GimmeMotifs package (version 0.13.1+216.g7f81a8a) (Bruse and Heeringen, 2018; van Heeringen and Veenstra, 2010) was used to scan for motifs in enhancer regions. The GC normalization setting in GimmeMotifs package was used to normalize the GC% bias in different enhancers. To correct for the bias of motif length, z-score normalization was performed on the motif scores. Normalization was done per motif, based on motif matches in random genomic regions using the same motif scan settings. The highest z-score was chosen if a TF had more than one motif. The enhancer intensity levels were scaled from 0 to 1, with 1 being the highest and 0 the lowest.

Gene regulatory network inference

The weighted sum of TF predicted enhancer intensity within 100kb around TSS is defined as the TF-gene binding score (Eq. 2). The distance weight is based on a linear genomic distance between the enhancer and the TSS of a gene according to equation 3.

$$B_{x,r} = \sum_k w_k s_k \qquad (2)$$

where $B_{x,r}$ is the binding score between TF x and target gene r, w_k is the weighted distance between an enhancer and the target gene and where s_k is predicted binding intensity at genomic position k of TF x. The distance weight calculation was similar to the method previously described in (Wang et al., 2016), except that only signal in enhancers is used, enhancers within 2kb around TSS are removed and the weight of enhancers within 2kb to 5kb is set to 1.

$$w_k = \begin{cases} 0, & k \in (0kb, 2kb] \\ 1, & k \in (2kb, 5kb] \\ \dfrac{2e^{-\mu|k-t_r|}}{1+e^{-\mu|k-t_r|}}, & k \in (5kb, 100kb] \end{cases} \qquad (3)$$

where t_r is the genomic position of the TSS of gene r and the parameter μ, which determines the decay rate as a function of distance from the TSS, is set such that an enhancer 10 kb from the TSS contributes one-half of that at the 2 kb to 5kb from TSS.

We scaled the expression level of the TF and the target gene, expressed as transcripts per million (TPM), and the TF-gene binding score $B_{x,r}$ we calculated in the first step from 0 to 1, with 1 being the highest and 0 the lowest. Combining the TF-gene binding score and TF and target expression scores by taking the mean, we obtained a TF-gene interaction score. Ideally, the contributions of these individual scores would be determined by a supervised method, such as a linear regression, however, due to the lack of a high-quality gold standard reference data set we chose to combine the scores through mean averaging.

Gene regulatory network evaluation

To evaluate the quality of the predicted GRNs, three different types of reference datasets were used: gene co-expression, Gene Ontology (GO) annotation (The Gene Ontology, 2019) and three regulatory interaction databases (RegNetwork (Liu et al., 2015), TRRUST (Han et al., 2017) and MSigDB C3 (Liberzon et al., 2011)). The expression correlation database was downloaded from COXPRESdb (Obayashi et al., 2019), and the original mutual rank correlation score was scaled to 0 to 1 for each TF, with 1 being the highest and 0 the lowest, and all scaled correlation score higher than 0.6 were considered as true interaction pairs. The human GO validation Gene Association File (GAF) (version 2.1) was downloaded from http://geneontology.org. We used all TF-gene pairs that were annotated with at least one common GO term as true positives. In each cell type, four types of cell type-specific reference datasets were selected from previously described reference datasets by only selecting only interaction for which both the TF and its target gene are expressed (TPM > 10 or TPM > 1) in the corresponding cell type. For the random network we used the same network interaction structure, but here we randomized the interaction score (the edge weight). The AUC of ROC and PR for each cell type GRN and corresponding random GRN were calculated.

Influence score inference

To calculate the influence score for the transition from a source cell type to a target cell type, we used the GRNs for both cell types. In each network, we selected the top 100k interactions based on the rank of its interaction score. We obtained a differential GRN by taking the interactions only located in the target cell type. The difference of the interaction score was used as the edge weight for the differential GRN.

Based upon the differential GRN a local network was built for each TF, up to a maximal number of three edges. Using equation (3), a target score was calculated for each node in the network, based on 1) its edge distance from the TF of interest, 2) the interaction score and 3) the change in expression between the source cell type and the target cell type.

$$N_x^s = \sum_{r \in V_t}^{s} |G_r^s| \frac{P_{x,r}^s}{L_{x,r}^s} \qquad (4)$$

Where $r \in V_t$ is each gene (r) in the set of nodes (V_t) that make up the local sub-network of TF x and $L_{x,r}^s$ is the level (or the number of steps) that gene r is away from TF x in the network s. Nodes located further from the TF have less effect on the target score. $P_{x,r}^s$ is the interaction score between TF x and target gene r and G_r^s, the expression score, is the log-transformed fold change of the expression of gene r.

The target score (N_x^s) for each TF is the sum of the scores from all the nodes in its local network. Nodes present in multiple edges are calculated only for the edge closet to the TF of interest. Self-regulating nodes are not considered. The target score and the G_r^s of each TF are scaled to 0 to 1, and the mean of them was defined as the influence score of this TF. Subsequently, all TFs are ranked by their influence score.

Regulatory profile analysis of human tissues

The RNA-seq data of 18 human tissues was downloaded from (https://www.proteinatlas.org/humanproteome/tissue) (Uhlen et al., 2010). The H3K27ac ChIP-seq data of all tissues were download from the ENCODE project: esophagus (ENCFF166HVM), skin (ENCFF166BMF), thymus (ENCFF829DSA), ovary (ENCFF178CUD), adrenal (ENCFF120ZSN), lung (ENCFF684FZC), spleen (ENCFF626HSF), skeletal (ENCFF082LKM), heart (ENCFF834ZEK), intestine (ENCFF410WCE), stomach (ENCFF972FYM), colon (ENCFF342MZW), pancreas (ENCFF015LEU), liver (ENCFF572NBX), prostate (ENCFF606FDW), cervix (ENCFF113QJM), bone (ENCFF835QFJ), and brain (ENCFF334MEF) (ENCODE Project Consortium, 2012). The gene expression score of each tissue was

calculated by taking the log2 TPM fold change between a tissue and the average of all other tissues. The GRN of each tissue was inferred using ANANSE. For prediction for TFs of one tissue, GRN interaction scores of all other tissues were averaged as the source GRN. All correlation analyses were clustered by hierarchical clustering method. The modular visualization of anatograms and tissues was done using the gganatogram package (version 1.1.1) (Maag, 2018).

Results

Cell type-specific transcription factors predominantly bind to enhancers

To systematically examine TF binding patterns in the genome in relation to cell type specificity, we downloaded the binding sites of 296 human TFs from the ReMap project, that re-analyzed all publicly available ChIP-seq data in various cell types and tissues (Chèneby et al., 2017). To determine the genomic distribution of these binding sites, we divided the genome into different genomic categories according to human UCSC known gene annotation (Hsu et al., 2006), and assigned binding sites to these categories based on the locations of the binding sites (Figure 1A). We grouped these categories into two main classes: 1) a promoter-proximal class, containing promoter (<=2kb), 5' UTR and 1st exon peaks, and 2) a promoter-distal class, referred to "Enhancers", containing all exons except the first, the 1st intron, other introns and intergenic categories. The percentage of TF binding sites in each genomic category was calculated, and TFs were ordered according to their percentages in the promoter-proximal class (Figure 1A) (Supplementary Table S4). We found that different TFs have a binding preference in either the promoter range or in the enhancer range (Figure 1A). However, the majority of TFs (77.5%) mainly bind in cis-regulatory regions that are distal from the promoter (Figure 1B). These binding sites will not necessarily all be functional, however, they are not close to gene promoters and contain the majority of the enhancers. For the purpose of this manuscript we will refer to them as enhancers.

To further dissect the binding pattern of cell type- or tissue-specific TFs, we performed Gene Set Enrichment Analysis (GSEA) (Sergushichev, 2016) on TF expression in different tissues. We defined tissue-specific TFs based upon the union of tissue enriched proteins, group enriched proteins, and tissue enhanced proteins as defined in human tissues from the Human Protein Atlas (Uhlén et al., 2015) (Figure 1C). GSEA showed that TFs mostly binding to enhancers are indeed enriched for tissue-specific expression (adjusted p value = 2.0e-4) (Figure 1C) (Supplementary Table S4). For example, SOX10 is a critical TF during neural crest and peripheral nervous system development (Kim et al., 2014), while TP63 is a master regulator in epithelial development (Soares et al., 2019). Both of these tissue-specific TFs showed a very high percentage of enhancer-binding, 93% for SOX10 and 82% for TP63 (Figure 1A).

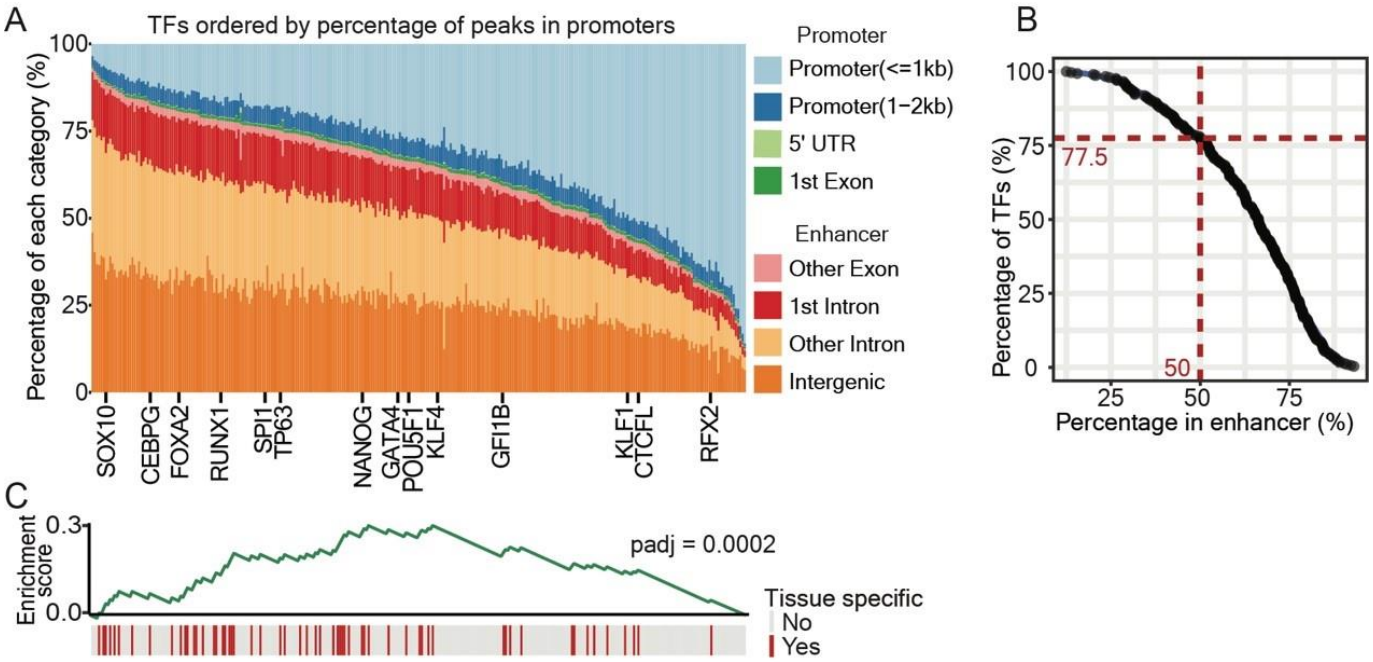

Figure 1. Tissue-specific TFs predominantly bind to enhancers. (A) Genomic location analysis of binding sites of 296 human TFs. The human genome was split into several categories: Promoter (<=1kb), Promoter (1-2kb), 5' UTR, and 1st Exon, Other Exons, 1st Intron, Other Introns, and Intergenic; these categories were further grouped into a promoter-proximal class (Promoter (<=1kb), Promoter (1-2kb), 5' UTR, and 1st Exon) and an enhancer class (Other Exons, 1st Intron, Other Introns, and Intergenic). The percentage of binding sites of each TF in different categories was calculated, and indicated with different colors. TFs were ordered by the percentage of binding sites within the promoter-proximal class. Several example TFs are marked at the bottom of the figure. **(B)** The percentage of TF binding sites in the enhancer class. 77.5% of TFs have 50% of its binding sites in the enhancer class of the genome. **(C)** Gene Set Enrichment Analysis (GSEA) on tissue-specific TFs and their enhancer binding. The red bars mark the tissue-specific TFs. The order of TFs is consistent with (A). Grey bars represent TFs that do not show tissue-specific gene expression. The GSEA enrichment score is represented by the green line (padj: 2.0e-4).

Taken together, our analysis of transcription binding sites revealed that most TFs, and specifically tissue-specific TFs, predominantly bind to cis-regulatory elements that are not proximal to gene promoters. This suggests that including enhancer information in computational methods for predicting key TFs in cell fate determination could be highly beneficial.

ANANSE: an enhancer network-based method to identify transcription factors in cell fate changes

Starting from the premise that the majority of TFs predominantly bind to enhancer regions, we developed ANANSE, a network-based method that uses properties of enhancers and their GRNs to predict key TFs in cell fate determination. As trans-differentiation is an ideal model for studying cell fate conversions controlled by key TFs, we set out to use this model to validate our computational approach. In the following paragraphs a conceptual overview of ANANSE is provided. Subsequently we will validate each of the steps involved.

First, we inferred cell type-specific TF binding profiles for each cell type. The input data of ANANSE consists of genome-wide measurements of enhancer activity (defined below), transcription factor motifs and expression data. We inferred the TF binding probability based on a supervised model that integrates the enhancer activity combined with TF motif scores. Second, we constructed cell type-specific GRNs based on the inferred TF binding probability and expression levels of predicted target genes (Figure 2B, 2C). The nodes in the network represent the TF or gene. The TF-gene interaction scores, represented by edges of the network, are calculated based on the predicted TF binding probability, the distance between the enhancer and the target gene, and expression of both TF and the target gene. By integrating these data, ANANSE determines the interaction score of each TF-gene pair.

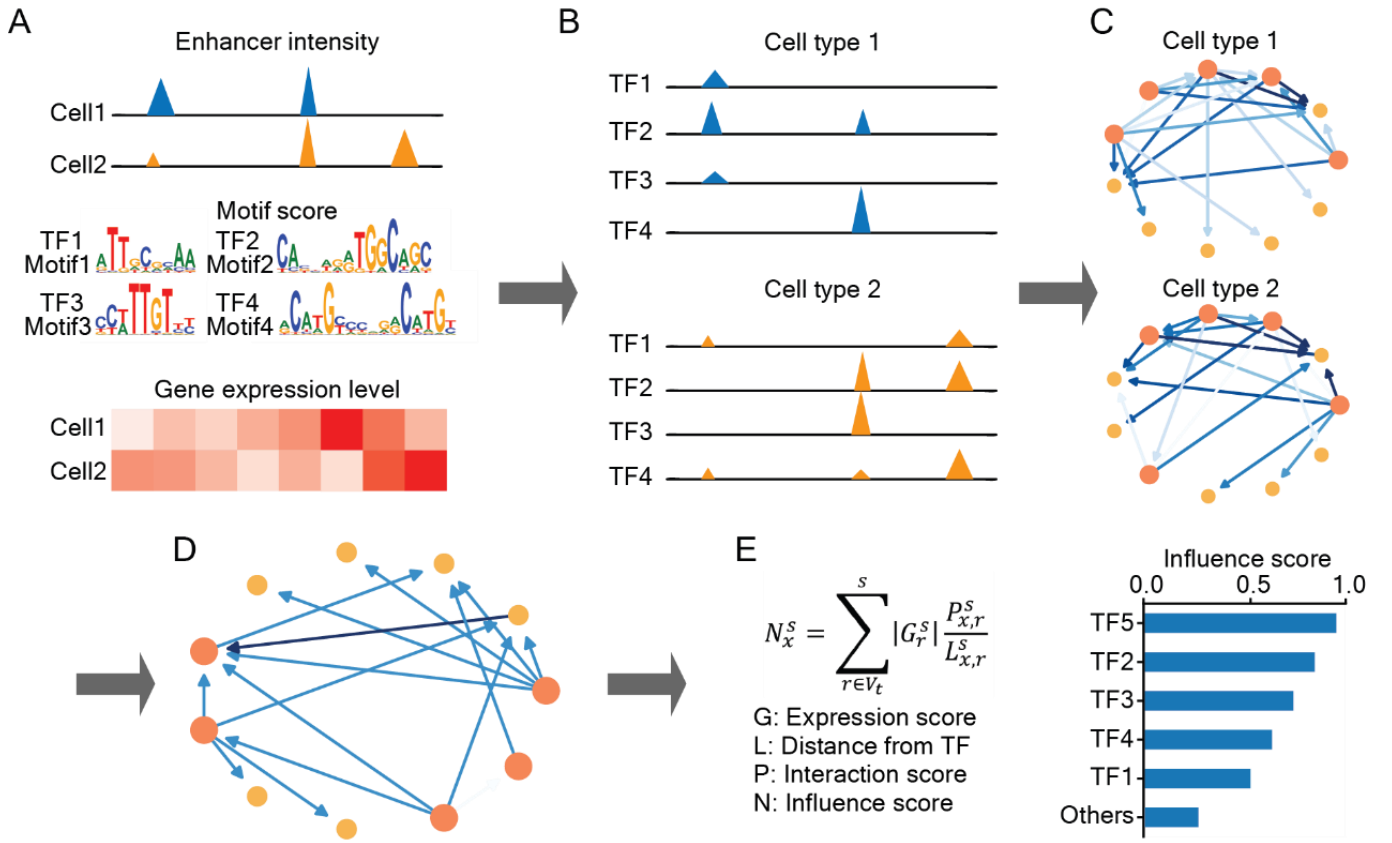

Figure 2. An overview of the workflow of the ANANSE method. (A) Data types used by ANANSE. These data include motif score of all TFs, gene expression data (e.g. RNA-seq) and enhancer data (e.g. H3K27ac ChIP-seq) from each cell type. The blue and orange peaks represent enhancers in two cell types. The four sequence logos represent the motifs of four TFs. The heatmap represents gene expression level in two different cell types. **(B)** The TF binding profiles predicted from the enhancer data and TF motif scores in each cell type. The two GRNs below show cell type-specific TF binding profiles in two cell types (source and target cell types). **(C)** The partial cell type-specific GRN predicted based on TF-Gene binding and TF/Gene expression. The two networks show cell type-specific GRNs in two cell types. The orange circle represents a TF or a gene, and the size of the circle indicates the target gene number of the corresponding TF. The color of the circle indicates the expression score of the corresponding TF. The blue arrow indicates regulation between two TFs, and the color intensity represents the relative strength of the predicted regulatory interaction. **(D)** The partial differential GRN between the two cell types. In this step, the interaction specific for the target cell type is kept constant, and if the interaction score of the target cell type is higher than that of the source cell type, the interaction score is further used. **(E)** The barplot shows the ranked influence score of all TFs calculated from the differential GRN. The influence score is calculated based on the gene expression score, the distance from the TF to the gene in the predicted network, and the interaction score between TF and gene.

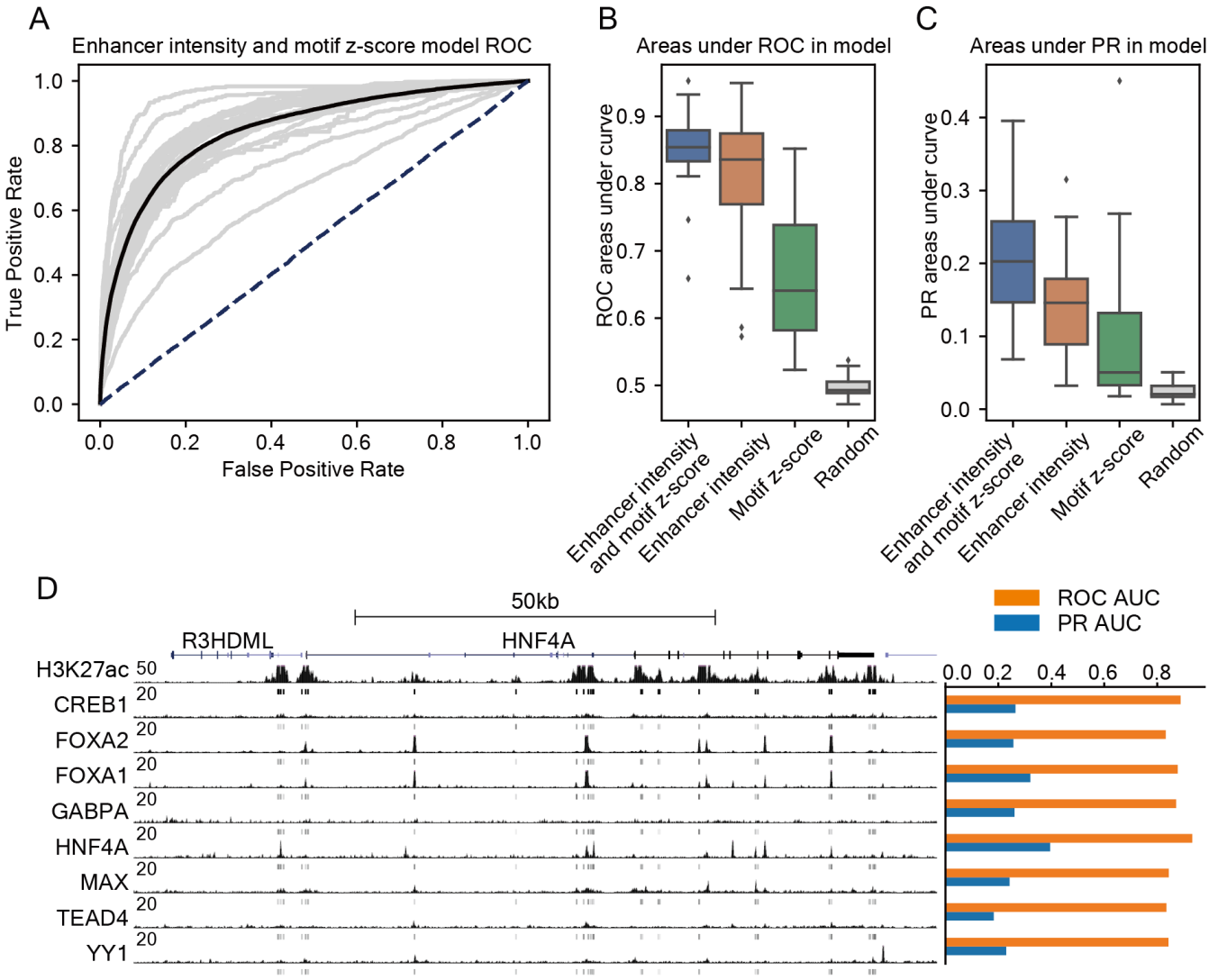

Figure 3. The performance of predicting TF binding sites using TF motif scores and enhancer activities. (A) Receiver-operator characteristic (ROC) curves representing the performance evaluation of the regression model in predicting genome-wide binding for 29 TFs. The ROC AUC score was calculated using leave-one-out cross validation. Each gray line represents the prediction of one TF, based on the model trained on all other 28 TFs. The black line indicates the mean prediction performance of all 29 TFs. **(B)** The prediction performance of the regression model (blue) compared to the baseline of enhancer signal (orange), motif z-score (red), and random data (green). The boxplot shows the ROC AUC of 29 TFS. **(C)** The same data as in B), quantified using the PR AUC. **(D)** A UCSC Genome Browser screenshot of predicted TF binding probability (gray bars) and ChIP-seq signals (black peaks) of eight TFs in the HepG2 cell line at the HNF4A gene locus. The ChIP-seq signals H3K27ac (top) from ENCODE in the HepG2 cell line is shown for comparison. The barplot on the right shows the ROC (orange) and PR (blue) AUC of four TFs, with the same order of TFs shown in ChIP-seq signals on the left.

Third, we used the GRN that is differential between two cell types to calculate the TF 'influence' score (Cahan et al., 2014; Rackham et al., 2016) (Figure 2D, 2E). This score represents a measure of importance of a TF in explaining transcriptional differences between the two cell types (Figure 2D, 2E). In this step, the difference in gene regulatory interactions represented by TF-gene interaction scores between the source and the target cell types is calculated.

The details of the algorithms are described in the following sections.

Transcription factor binding can be predicted by the motif score in combination with the enhancer activity

Sequence-specific TFs bind to their cognate DNA motifs in the genome and activate or repress their target genes. To infer the target genes of a TF, the genomic binding sites of this TF are informative. ChIP-seq has been broadly used to identify TF binding sites at genome-wide scale. However, it is unfeasible to perform ChIP-seq for every TF in all cell types, e.g. due to the availability and quality of the TF antibodies. Therefore, it would be highly beneficial to be able to predict binding sites of individual TFs in a given cell type.

Here, we used a conceptually simple general logistic regression model to predict TF binding sites based on the TF motif z-score and the enhancer activity (see Methods for details). Our model uses a predefined set of putative enhancers. These can be based on genome-wide measurements that provide relatively accurate estimates of enhancer locations, such as transcription factor ChIP-seq, ATAC-seq or DNase-seq. In this work, we used a set of putative enhancer regions based on an integration of all TF ChIP-seq peaks from ReMap 2018 (Chèneby et al., 2017). The enhancer activity is based on the number of H3K27ac ChIP-seq reads in 2kb regions centered at the enhancer summit. For each enhancer, we scanned for motifs in a 200bp region centered at the peak summit using GimmeMotifs (Bruse and Heeringen, 2018; van Heeringen and Veenstra, 2010).The motif z-score was calculated by GimmeMotifs with the GC%-normalization option. The log-odds score based on the positional frequency matrix is normalized by using the mean and standard deviation of scores of random genomic regions. These random regions are selected to have a similar GC% as the input sequence.

To train and evaluate our model, we created a reference of putative enhancers based on integrating the summits of all transcription factor peaks from ReMap 2018 (see Methods for details) (Chèneby et al., 2017). Additionally, we used ENCODE H3K27ac ChIP-seq data from the five cell types (GM12878, hESC, HeLa-S3, HepG2 and K562) to represent enhancer activities in our method. We used ChIP-seq peaks of 28 TFs from the ENCODE-DREAM in vivo Transcription Factor Binding Site Prediction Challenge (https://www.synapse.org/ENCODE) as evidence of TF binding. The ChIP-seq data from this challenge has been consistently processed using the ENCODE pipelines (Davis et al., 2018) (Supplementary Table S5). We examined the locations of the TF peaks by overlapping with our enhancer reference, and only the subset of peaks that overlapped with these enhancer regions was kept for further analysis (see Methods for details).

To test the prediction performance of our model, we established a leave-one-out cross-validation procedure. We excluded each TF in turn for testing, and trained the model on the remaining 27 TFs. In addition, for all evaluations we trained on all chromosomes except chr1, chr8 and chr21 and used those as a validation dataset to evaluate the predictions. This makes the training procedure consistent with the ENCODE-DREAM challenge. Using the trained model, we evaluated whether binding of the test TF was correctly predicted in the five cell types. We evaluated the performance of the model using the AUC (Area Under Curve) of the ROC (Receiver Operating Characteristic) (Supplementary Table S5). The median ROC AUC of all 28 TFs was 0.85, which is significantly higher than expected by random chance (AUC = 0.5) (Figure 3A, Supplementary Figure S1). In addition, the regression model outperforms the baseline of enhancer intensity and motif z-score (Figure 3B, Supplementary Figure S1). Generally, ROC curves are appropriate when the observations are balanced between groups, however, they can be misleading in the case of unbalanced data (Saito and Rehmsmeier, 2015). Therefore, we calculated the PR AUC score for the binding prediction of all 28 TFs, which shows a similar pattern as the ROC AUC. The median PR AUC of the model (0.20) is significantly better than both the random situation (median 0.02) and the motif z-score alone (median 0.05) (Figure 3C, Supplementary Figure S1) (Supplementary Table S5). For comparison to methods that train supervised transcription factor-specific models, such as the ENCODE-DREAM entries, we also validated our model on the validation chromosomes (chr1, chr8, and chr21) in the ENCODE-DREAM validation cell types (liver, MCF7, PC-3, K562, and iPS). As a comparison, we used the Virtual ChIP-seq predictions (Karimzadeh and Hoffman, 2019). This is a newly developed supervised artificial neural network method to predict individual TF binding, which shows comparable results compared to the top ENCODE-DREAM entries. As expected, our model outperforms a simple motif scoring approach, but it does not perform as well as the transcription factor-specific Virtual ChIP-seq method (Supplementary Figure S2). For instance, the CTCF binding predictions for Virtual ChIP-seq are significantly better. However, this factor is not expected to influence enhancer activity as measured by H3K27ac, which is a component of our model. The main advantage of the model implemented in ANANSE is that it does not depend on a large quantity of high-quality ChIP-seq data being available for every factor. This is important for TFs for which no good antibody exists, but also for application in any species that does not have the abundance of training data provided by ENCODE for mouse and human.

An example of binding site predictions of several TFs at the HNF4A locus in HepG2 cell line is shown in Figure 3D, which demonstrates that our method is able to predict most TF binding sites where strong enhancer signals are present. These analyses illustrated that we established a TF binding site prediction method, which can be applied on the basis of one experimental measurement (H3K27ac ChIP-seq) and yields more accurate predictions than a purely motif-based approach.

ANANSE predicts cell type-specific gene regulatory networks

Using the inferred cell type-specific binding profiles, we sought to determine the interactions of TFs and their target genes (TF-gene) to establish cell type-specific GRNs. To calculate the TF-gene interaction score we first identified all enhancers for each gene. In our TF binding prediction model, we used H3K27ac ChIP-seq as training data. Here, we used our ReMap-based enhancer reference to provide enhancer locations. The enhancer activity is based on the number of H3K27ac reads in 2 kb centered at the enhancer.

For each gene, we took all enhancers that are located at least 1kb from the gene TSS and within a maximum distance of 100 kb. Subsequently, the strength of a TF-gene interaction in the network was defined by the sum of the predicted TF binding strength in all identified enhancers of the target gene, weighted by the distance (Figure 4A). The distance weight was calculated from the linear genomic distance between the enhancer and the TSS of a gene, such that distal enhancers receive a low weight and nearby enhancers have a high weight (Wang et al., 2016) (Figure 4A). This model resulted in a TF-gene binding score, indicating the TF-target gene binding intensity for all combinations of TFs and target genes pairs.

The original idea of the ANANSE method is to use genome-wide measurements of enhancer activity, such as ChIP-seq of H3K27ac, as input to predict cell type-specific activation GRN. Based on the assumption that the interaction of every TF-gene pair in a specific cell type is proportional to their relative

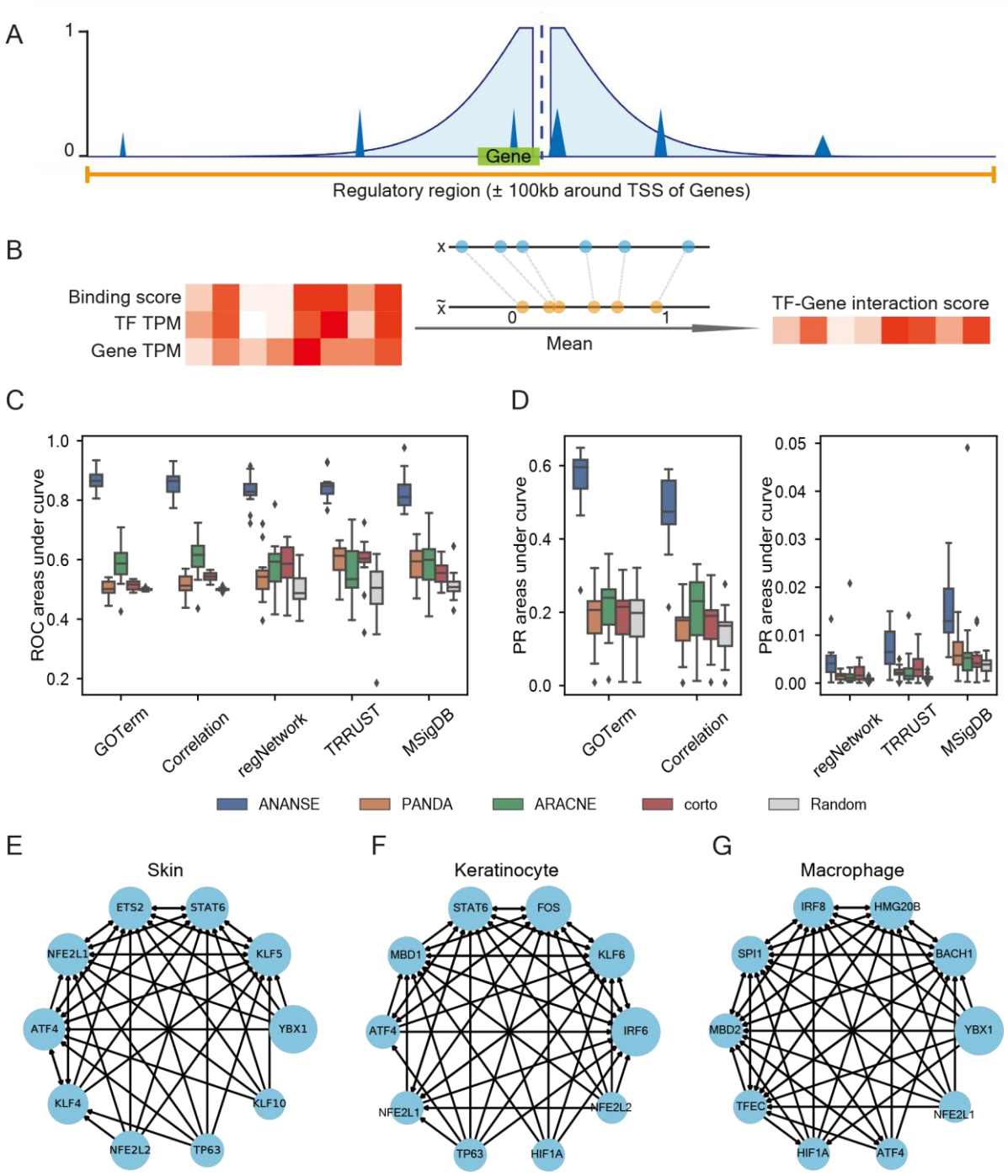

Figure 4. Prediction of cell type-specific enhancer gene regulatory networks. (A) A schematic overview of the calculation of TF-Gene binding score from the predicted binding intensity of TFs. The green rectangle represents one target gene and the orange line shows 100kb up- and downstream of the TSS of the corresponding gene, the range that is used to include enhancers for calculation. The dark blue triangles represent all predicted TF binding peaks within the 100kb range around the gene. The height of the shaded light blue area represents the weight calculated based on the linear genomic distance from TSS of the target gene to the enhancers. For example, the distance weight for the distance of 1kb from the TSS is 1, and for the distance of 100kb from the TSS is 0 (Wang et al., 2016). **(B)** A schematic overview of the calculation of the TF-Gene interaction score. The heatmaps on the left represent the TF-Gene binding score, TF expression level (TPM) and target gene expression level (TPM) of each TF-Gene regulatory pair. All three scores are scaled from 0 to 1, and the mean of three scores of each TF-Gene pair is defined as the interaction score (right heatmap) of the corresponding TF-Gene pair. **(C)** Evaluation of the predicted networks using different types of data: a gene ontology (GO) term co-regulatory network, a cell type-specific gene correlation network, and three TF-Gene regulatory networks based on interaction databases (regNetwork, TRRUST, and MSigDB C3). The boxplots show the AUC of ROC for 15 different tissues. ROC AUC of the ANANSE predicted networks is shown in blue; the PANDA networks in orange; the ARACNE networks in green; the corto networks in red; the random networks in gray. **(D)** The same evaluation as in C), with the PR AUC shown as a boxplot. **(E)** Example network predicted for skin. The blue circles show the top 10 TFs in this cell type. The size of the circle indicates the target gene number of the corresponding TF. The black arrows indicate the interaction score between the two TFs. **(F)** Example network predicted for keratinocytes, visualized as in E). **(G)** Example network predicted for macrophages, visualized as in E).

expression, we included the expression level of the TF and the target gene. We scaled the expression level of the TF and the target gene, initially expressed as transcripts per million (TPM), to a normalized expression of 0 to 1, with the lowest expression as 0 and highest as 1. Combining the TF-gene binding score and TF and target expression scores by taking the mean, we obtained a TF-gene interaction score that represents the predicted strength of the TF-gene regulation (Figure 4B). Together, all TF-gene interaction scores represent a cell type-specific GRN.

To evaluate the quality of the inferred GRNs, we used three different types of reference datasets: gene co-expression, Gene Ontology (GO) annotation (The Gene Ontology, 2019) and regulatory interaction databases containing known TF-target gene interactions. We downloaded co-expression data for human genes from the COXPRESdb database (Obayashi et al., 2019). All TF-gene pairs with a correlation >= 0.6 were used as true positives. For the GO validation set, we used TF-gene pairs that were annotated with at least one common GO term as true positives. Finally, we used the TF-gene interactions from three databases of regulatory interactions, RegNetwork (Liu et al., 2015), TRRUST (Han et al., 2017) and MSigDB C3 (Liberzon et al., 2011). RegNetwork is an integrated database of transcriptional and post-transcriptional regulatory networks in human and mouse, TRRUST is an expanded reference database of human and mouse transcriptional regulatory interactions, and MSigDB C3 is a collection of gene sets that represent potential targets of regulation by TFs.

We evaluated cell type-specific GRNs predicted by ANANSE and compared them with other published methods in 15 tissues: adrenal gland, bone marrow, brain, cervix, colon, esophagus, heart, liver, lung, ovary, pancreas, prostate, skeletal muscle, skin, small intestine, spleen, and stomach. As the previously described reference datasets contain regulatory interactions for all genes, regardless of cell type, we created high confidence cell type-specific reference data by filtering for TFs and genes that are expressed, using a stringent cutoff of TPM > 10. As comparison, we included three GRN inference methods that were used to create tissue-specific networks using GTEx expression data: PANDA (Glass et al., 2013), ARACNE (Margolin et al., 2006), and corto (Mercatelli et al., 2020).

To compare with the other tissue-specific GRN inference methods, we selected the overlapping network edges among four predicted methods in each tissue. We first evaluated the models by calculating the AUC of the ROC using the different reference sets for the 15 tissues (Figure 4C). For the ANANSE networks, the mean AUC ranges from 0.82 using the MSigDB C3 to 0.87 using the GO term database while the median AUC of randomized networks is close to 0.5 (Figure 4C). When we compared with other published GRN inference methods, all three methods show a significantly lower AUC. The ARACNE method has a highest mean AUC of 0.60 using the co-expression database; the PANDA method has a highest mean AUC of 0.59 using the TRRUST database and the corto method has a highest mean of AUC 0.59 using the TRRUST database (Figure 4C). Some of the reference databases contain very few interactions (the positives in this evaluation) as compared to all possible interactions (which determine the negatives). For instance, the fraction of positive interactions is 0.09% in TRRUST, 0.07% in RegNetwork, and 0.33% in MSigDB C3. Therefore, we also evaluated the predicted networks using the PR AUC (Figure 4D). In absolute terms, the PR AUC is considerably lower than the ROC AUC, especially for the TRRUST, RegNetwork, and MSigDB C3 reference sets (mean PR AUC of 0.0072, 0.0045, and 0.0154, respectively), but for all tissues there is a relatively large and statistically significant difference between the predicted GRN and the random network (p-value = 3.27e-4) (Figure 4D). The expression-based networks of the other three published methods show significant lower mean PR AUC when compared with ANANSE for all five different types of reference datasets (Figure 4D). We also repeated the evaluation with a lower cutoff TPM >1 for both TFs and target genes, which does not change the interpretation of the results (Supplemental Figure S3 A and B). When we compared the networks inferred by ANANSE with those predicted by the three published methods, we used only the overlapping network edges among the four predicted GRNs. We also repeated those analysis with the union of all interactions among the four predicted GRNs, and set the missing interactions as 0. This shows similar results with both a higher reference cutoff TPM >10 (Supplemental Figure S3 C and D) and lower reference cutoff TPM >1 (Supplemental Figure S3 E and F) of TFs and target genes.

To qualitatively assess the cell type-specific GRNs predicted by ANANSE, we chose one tissue (skin) and two well-studied cell types (epidermal keratinocyte and macrophage), and constructed their GRNs using the top ten predicted TFs of each cell type, as ranked by outdegree. The GRN of both skin and keratinocyte includes TFs that are known to regulate keratinocyte proliferation and epidermal differentiation, such as KLF5, KLF6 and TP63 (Figure 4F) (Nair et al., 2006; Oberbeck et al., 2019; Richardson et al., 2006; Sen et al., 2012; Tsuji et al., 2018). The GRN of macrophage contains classical macrophage marker genes and reprogramming factors, such as SPI1 (Figure 4E) (Feng et al., 2008; Xie et al., 2004).

Taken together, our benchmarks and examples demonstrate that GRNs generated by ANANSE allow for meaningful cell type-specific prioritization of TFs.

ANANSE accurately predicts key transcription factors for trans-differentiation

Having established that ANANSE-inferred GRNs can enrich for biologically relevant regulatory interactions, we aimed to use these GRNs to identify key TFs that regulate cell fate determination. To this end, trans-differentiation is a good model for this purpose, as experimentally validated TFs have been determined for various trans-differentiation strategies. Here, we first inferred the GRNs for all cell types using our ANANSE approach. The ANANSE-inferred GRN differences between two cell states, a *source* cell type and a *target* cell type, was calculated to represent the differential GRN between two cell types, which contains the GRN interactions that are specific for or higher in the target cell type. Subsequently, using an approach inspired by Mogrify (Rackham et al., 2016), we calculated the influence score of TFs for these trans-differentiations by determining the differential expression score of its targets weighted by the regulatory distance (see Methods for details).

To evaluate the prediction by ANANSE, we used experimentally validated TFs for several trans-differentiation

Table 1. The summary of seven experimentally validated trans-differentiations from fibroblast to target cell types

Target cell type	Experimentally validated TFs	TFs predicted by ANANSE	Reference
Astrocyte	NFIA, NFIB, SOX9	NFIA, SOX9	(Caiazzo et al., 2015)
Cardiomyocyte	GATA4, MEF2C, TBX5	GATA4	(Fu et al., 2013)
	HAND2, NKX2-5, GATA4, MEF2C, TBX5	NKX2-5, GATA4	(Ifkovits et al., 2014)
Hepatocyte	ATF5, PROX1, FOXA2, FOXA3, HNF4A	HNF4A, ATF5	(Nakamori et al., 2017)
	FOXA1, FOXA3, HNF4A	HNF4A	(Simeonov and Uppal, 2014)
iPSC	SOX2, POU5F1, KLF4, MYC	SOX2, POU5F1	(Takahashi et al., 2007)
	POU5F1, SOX2, NANOG, LIN28	POU5F1, SOX2	(Yu et al., 2007)
	POU5F1, SOX2	POU5F1, SOX2	(Huangfu et al., 2008)
Keratinocyte	TP63, GRHL2, TFAP2A, MYC	TP63, TFAP2A	(Kurita et al., 2018)
Macrophage	CEBPA, CEBPB, SPI1	CEBPA, SPI1	(Xie et al., 2004)
	SPI1, CEBPA, CEBPB	CEBPA, SPI1	(Feng et al., 2008)
Osteocyte	RUNX2	RUNX2	(Li et al., 2017)
	RUNX2, POU5F1, MYCL	RUNX2	(Yamamoto et al., 2015)

strategies. For this, we collected TFs for seven trans-differentiation strategies with fibroblasts as the source cell type. The target cell types include astrocytes (Caiazzo et al., 2015), cardiomyocytes (Fu et al., 2013; Ifkovits et al., 2014), hepatocytes (Nakamori et al., 2017; Simeonov and Uppal, 2014), iPSCs (Huangfu et al., 2008; Takahashi et al., 2007; Yu et al., 2007), keratinocytes (Kurita et al., 2018), macrophages (Feng et al., 2008; Xie et al., 2004), and osteocytes (Li et al., 2017) (Table 1). We used H3K27ac ChIP-seq data of these cell types to create cell type-specific GRNs, and then calculated TF influence scores and ranked the TFs in each cell type.

When we calculate TF influence scores from cell type-specific GRNs, it is important to decide what size of GRN should be chosen in terms of the top number of edges. We inferred the key TFs for the seven trans-differentiations using six different sizes of GRNs (10K, 50K, 100K, 200K, 500K, and 1M edges) (Supplementary Figure S4). Supplementary Figure S5 show the average of the percentage of all known (experimentally validated) cell-fate determinants that are recovered as a function of the number of top predictions that are included. These results show that using a GRN size of 100K or 200K interactions results in the best recovery ability. Therefore, we chose a GRN size of 100K interactions for all following analyses.

In all seven cases, many of the experimentally defined TFs are included in the top 10 factors predicted by ANANSE (Table 1). For example, ANANSE predicts CEBPA and SPI1 for reprogramming fibroblasts to macrophages (Feng et al., 2008; Xie et al., 2004) and ATF5 and HNF4A for reprogramming to hepatocytes, which is consistent with the experimental trans-differentiation strategies (Nakamori et al., 2017; Simeonov and Uppal, 2014).

As cell type-specific TFs predominantly bind to enhancers (Figure 1), and the inclusion of enhancer information is one of the unique features of ANANSE, we anticipated that ANANSE would have more accurate predictions of TFs for trans-differentiation. To investigate this, we compared the enhancer-based approach of ANANSE with a promoter-based model, which does not take into account promoter-distal regulatory elements, and with a model based on only gene expression data (Figure 5A). We created both expression and promoter based GRNs of the seven source and target cell type combinations. For expression-based GRNs, we used only the mean of the scaled TPM of TFs and genes together as the interaction score of TFs and genes. For the promoter-based GRNs, we selected the highest binding score of TFs within 2kb of the TSS of the corresponding gene as the binding score of the TF-gene pair. Subsequently, the mean of the scaled TPM of the TF and the gene together with the binding score determines the interaction score of the TF and gene (Figure 4B). We then inferred the key TFs for the seven trans-differentiations using ANANSE and these two types of GRNs. The ANANSE influence score based on the enhancer GRNs includes 46% of the known TFs in the top four predictions (Supplementary Figure S5 and Supplementary Table S6). In contrast, using the influence score based on the promoter GRN or the expression GRN, we could recover only 12% and 15% of the known TFs in the top four predictions (Figure 5A and Supplementary Figure S5). These results demonstrate that using enhancers in the construction of GRNs significantly improves the prediction of relevant TFs in cell fate determination.

Next, we further quantified the performance difference between ANANSE and previously reported methods, namely, Mogrify, CellNet, Lisa and the method of D'Alessio et al (Cahan et al., 2014; D'Alessio et al., 2015; Qin et al., 2020; Rackham et al., 2016) (Figure 5B and Supplementary Figure S6). For Mogrify, we downloaded both the prioritized list of TFs based on TF expression in source cell types and GRN overlap, as well as the full unfiltered list of TFs. For these comparisons, we aimed to include all seven trans-differentiation strategies. In some cases, as data for the exact cell type is unavailable, similar cell or tissue types were used as surrogates. For example, the osteoblast-Sciencell was used to substitute for osteoblast. For CellNet, we used the previously described results of three cell types: hepatocytes, iPSCs and macrophages (Rackham et al., 2016). For Lisa, we used the top 500 differentially expressed genes from fibroblast to each target cell types as input (Qin et al., 2020). For all methods, the resulting transcription factors were ranked according to the relevant output score of the method. Using the seven cell type conversions as a reference,

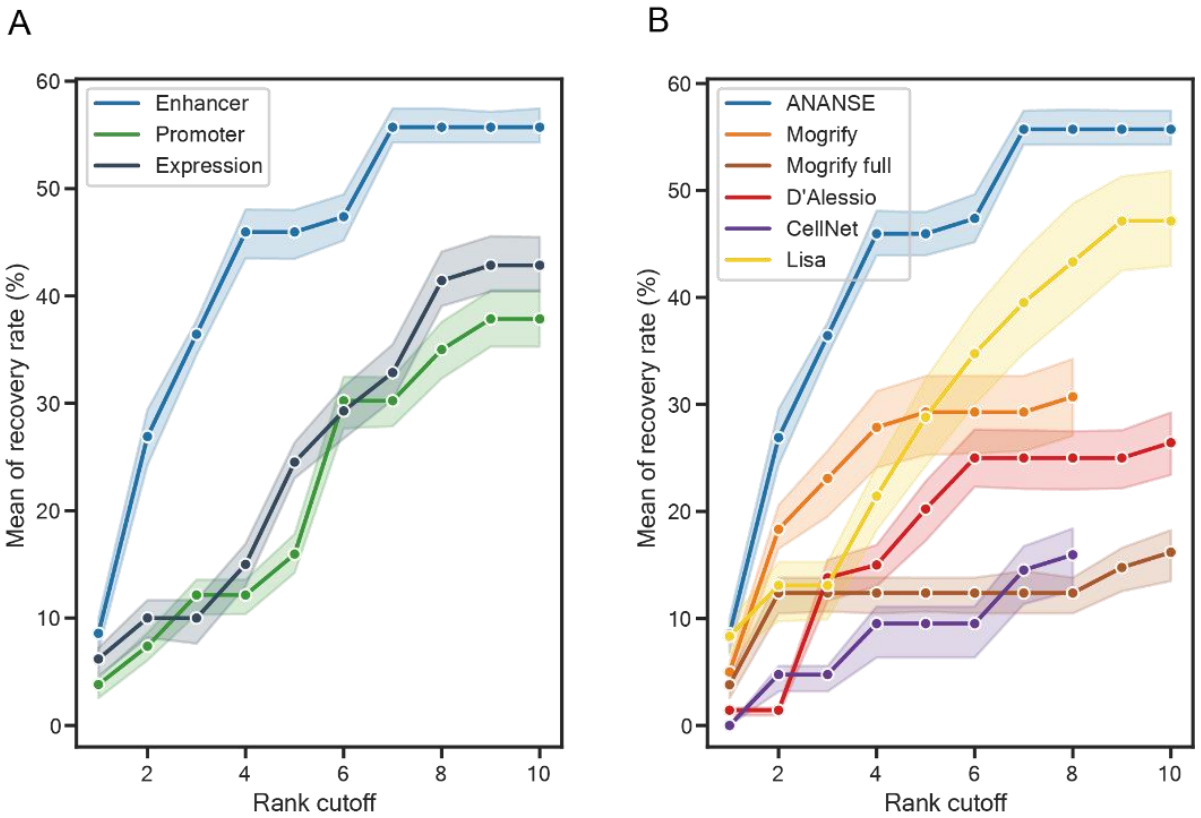

Figure 5. Evaluation of the performance of ANANSE using experimentally validated trans-differentiation strategies. (A) The line plots show the comparison of the predicted top TFs for trans-differentiation from cell type-specific networks. Based on the difference between two networks, TFs were prioritized using the influence score calculation implemented in ANANSE. Shown is the fraction of predicted TFs compared to all known TFs based on trans-differentiation protocols described in the literature (y-axis) as a function of the top number of TFs selected (x-axis). The mean of recovery rate is the average of all TF sets when corresponding trans-differentiation has several different experimentally validated TF sets. The shaded area represents the minimum and maximum percentage of corresponding recovered TFs when using six out of seven trans-differentiations. Three different types of networks were used: gene expression (deep blue), promoter-based TF binding in combination with expression (green), and enhancer-based TF binding in combination with expression (blue). **(B)** The line plots show the comparison of the predicted top TFs for trans-differentiation based on different computational methods. The y-axis indicates the percentage of experimentally validated cell TFs that are recovered as a function of the number of top predictions, similar as in A). Six different methods are shown: ANANSE (blue), Mogrify (orange), Mogrify without using their selection algorithm (brown), the method of d'Alessio et al. (red), CellNet (purple) and Lisa (gold). The shaded area represents the minimum and maximum percentage of corresponding recovered TFs when using six out of seven trans-differentiations. CellNet only contains data from fibroblast to ESC, Hepatocyte, and Macrophage; and Mogrify and CellNet only contain the top 8 predicted factors.

ANANSE has the highest recovery at all rank cutoffs up to 10 (Figure 5B and Supplementary Figure S6). ANANSE predicts a mean of 46% TFs using the top four TFs ranked by influence score, while other methods predict a maximum of 28% TFs with this rank cutoff (Figure 5B and Supplementary Figure S6). When the number of predicted TFs was increased to ten, ANANSE could increase its recovery rate to 56%, while the maximum mean recovery of other methods is 47% (Figure 5B and Supplementary Figure S6).

In summary, these analyses show that including enhancers in the GRN construction significantly improves the prediction TFs in cell fate conversion and that ANANSE outperforms other established methods, based on experimentally validated trans-differentiation TFs. Our results demonstrate that ANANSE can accurately prioritize TFs in cell fate determination.

ANANSE identified an atlas of key transcription factors in normal human tissues

The gene expression programs that drive the cellular differentiation programs of different tissues are largely controlled by TFs. To find out which key TFs drive cell fate determination in different tissues, we applied ANANSE to human tissue data. We downloaded H3K27ac ChIP-seq data as a measure of enhancer activity for 18 human tissues from the ENCODE project (ENCODE Project Consortium, 2012) and the RNA-seq data of corresponding tissues from the Human Protein Atlas project (Uhlén et al., 2015). Using these enhancer and gene expression data, we constructed tissue-specific GRNs using ANANSE, and then calculated the TF influence scores for each of the tissues when taking the combination of all other tissues as the source tissue (Supplementary table S7). We clustered the 18 tissues based on the correlation between TF influence scores using hierarchical clustering, showing that the

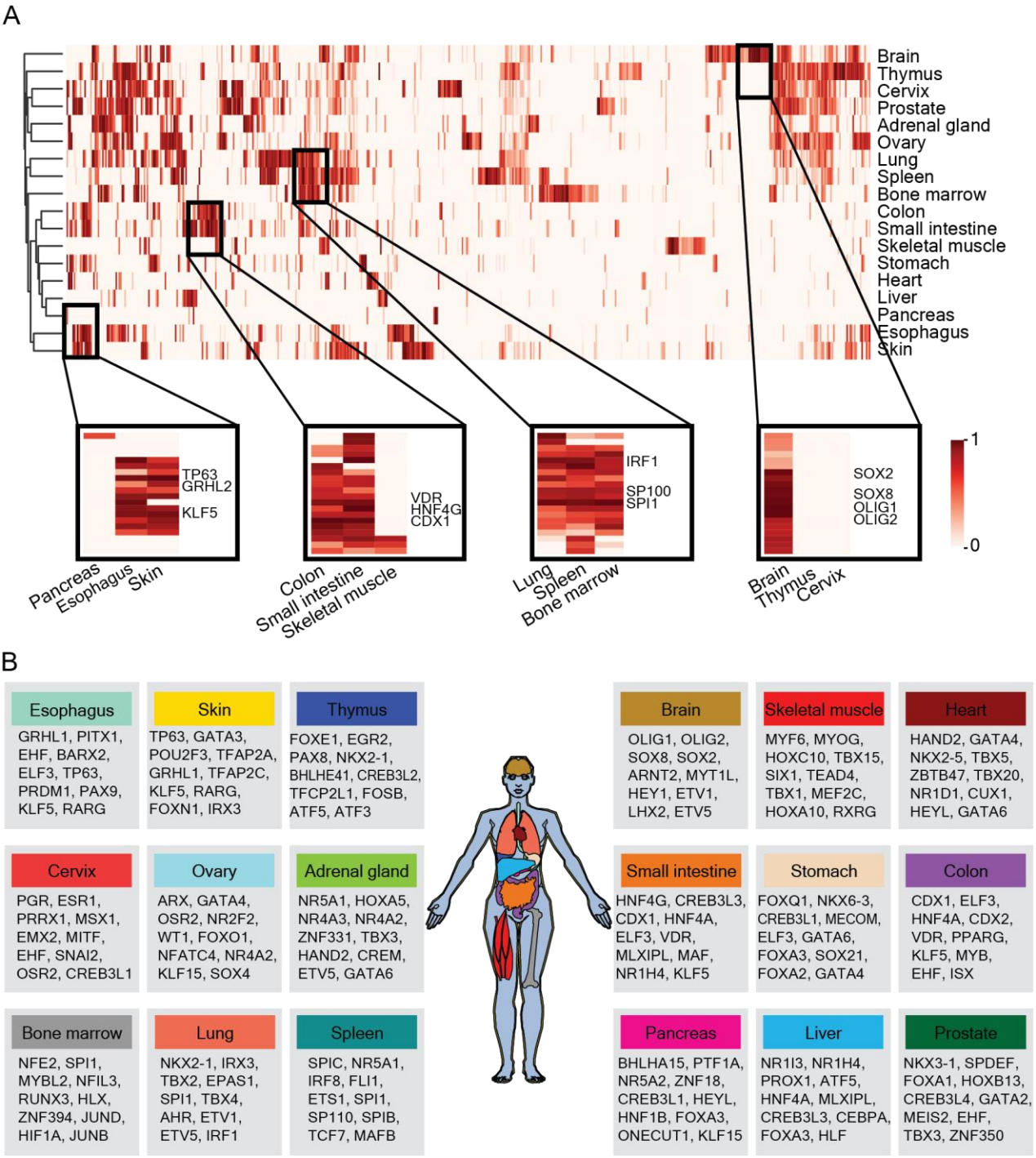

Figure 6. Applying ANANSE to expression data of human tissues to identify key transcription factors. (A) Heatmap of the predicted influence scores of all TFs using ANANASE on data from 18 human tissues. The color in the heatmap indicates the relative influence score, from low to high. The four small heatmaps highlighted below show important TFs in related tissues. **(B)** The top 10 key TFs of 18 tissues inferred by ANANSE. The color of the tissue is consistent with the tissue name in the box. The order of TF of each tissue is based on the influence score of the TF ranked from high to low.

influence score captures regulatory similarities and differences between tissues (Figure 6A and Supplementary Figure S4). For example, the esophagus and the skin cluster together, as these tissues are composed mostly of stratified squamous epithelial cells, and skeletal muscle and heart tissue are clustered together as both tissues contain striated muscle tissues.

For all studied tissues, we have provided a rich resource of key TFs of each tissue, with a list of top ten key TFs (Figure 6B). Many TFs in this list are known to play important functions for specific tissues, e.g. ELF3 and KLF5 for stomach, colon, and small intestine (Jedlicka et al., 2008; Katz et al., 2002); TP63 and GRHL1 for the skin and esophagus (Dollé, 2009; Qu et al., 2018; Wilanowski et al., 2008); SOX2, SOX8 and OLIG1/2 for brain (Bani-Yaghoub et al., 2006; Meijer et al., 2012; Muto et al., 2009); and SPI1 and IRF1 for lung, spleen and bone marrow (Ohteki et al., 2001) (Figure 6A).

The gastrointestinal tract tissues share a number of highly influence score TFs such as ELF3, KLF4, and HNF4A, which play roles in stomach, colon, and small intestine development, and are consistent with the current research on gastrointestinal tract tissues (Figure 6A) (Jedlicka et al., 2008; Katz et al., 2002; Thompson et al., 2018). ELF3 is important in intestinal morphogenesis, homeostasis, and disease (Jedlicka et al., 2008). KLF4 is required for terminal differentiation of goblet cells in the colon (Katz et al., 2002).

Our analysis showed that TP63, TFAP2A, TFAP2C, RARG, and GRHL1 are common important TFs in the skin and esophagus (Figure 6B). The function of these TFs has been well studied in the skin. TP63 is one of the TFs that is important in both skin and esophagus development (Daniely et al., 2004; Kurita et al., 2018; Qu et al., 2018). TP63 and TFAP2A have been used in *in vivo* reprogramming of wound-resident cells to generate skin epithelial tissue (Kurita et al., 2018). Both TFAP2A and TFAP2C are required for proper early morphogenesis and development as well as terminal differentiation of the skin epidermis (Budirahardja et al., 2016; Kousa et al., 2018; Wang et al., 2008). GRHL1 is important for the functioning of the epidermis. Grhl1 knockout mice exhibit palmoplantar keratoderma, impaired hair anchoring, and desmosomal abnormalities (Wilanowski et al., 2008). It would be interesting to investigate how they play roles in esophagus. RARG is expressed in the developing skin epithelium, as well as in all prospective squamous keratinizing epithelia, including the esophagus and left wall of the stomach (Dollé, 2009; Ruberte et al., 1990). PAX9 regulates squamous cell differentiation and carcinogenesis in the oro-oesophageal epithelium (Xiong et al., 2018).

In summary, using ANANSE, we predicted key TFs for 18 human normal tissues. Many of these predicted TFs correlate well with the known literature of these tissues. In addition, the predicted key TFs in each tissue also provide us a rich resource to unveil novel TFs in specific tissues.

Discussion

Lineage specification and cell fate determination are critical processes during development. They are necessary to form the diversity of cell types that are organized into organs and tissues. TFs form a central component in the regulatory networks that control lineage choice and differentiation. Indeed, cell fate can be switched *in vitro* through manipulation of TF expression (Caiazzo et al., 2015; Fu et al., 2013; Kurita et al., 2018; Li et al., 2017; Simeonov and Uppal, 2014; Takahashi et al., 2007; Xie et al., 2004). However, the regulatory factors that determine cell identity remain unknown for many cell types. To address this issue, we developed ANANSE, a new computational method to predict the key TFs that regulate cellular fate changes.

We established TF binding networks for each cell type by leveraging genome-wide, cell type-specific enhancer signals from H3K27ac ChIP-seq data and TF motif data. ANANSE takes a two-step approach. First, TF binding is imputed for all enhancers using a TF-agnostic model. In contrast to existing methods that aim to predict binding by training TF-specific models (Batsis et al., 2019; Keilwagen et al., 2019; Li et al., 2019; Quang and Xie, 2019), we used a more general model that can be applied to all TFs. Logically, our model will be less accurate in predicting TF binding, as compared to models specifically trained for individual TFs. Indeed, the PR AUC and ROC AUC of the ANANSE binding model are lower than the current state-of-the-art in supervised prediction, as illustrated by the comparison with Virtual ChIP-seq (Karimzadeh and Hoffman, 2019). However, the advantage of our model is that it can predict binding for every TF as long as its motif is known. In addition, it can be used for factors for which there is no training data available, and for instance, it can also be applied to non-model organisms that lack comprehensive ChIP-seq assays. Our benchmarks show that it performs significantly better than using the motif score alone. We found that the enhancer signal intensity is the most important predictive feature for binding (Figure 3A-C and Supplementary Figure S1). The TF-specific motif z-score modestly increases the performance.

Second, we summarized the imputed TF signals per gene, using a distance-weighted decay function (Wang et al., 2016), and combine this measure with TF and target gene expression to infer cell type-specific GRNs. In general, there is a lack of gold standards to evaluate cell type-specific GRNs. To evaluate the GRNs, we used orthogonal types of benchmarks: a database of known, experimentally identified TF-gene interactions and functional enrichment using Gene Ontology annotation. The databases with known interactions that we used (TRRUST (Han et al., 2017) and regNetwork (Liu et al., 2015)) contain only a fraction of true regulatory interactions, and therefore this benchmark is affected by a large fraction of false negatives. All our benchmark evaluations demonstrate that ANANSE significantly enriches for true regulatory interactions. However, it also highlights that GRN inference is far from a solved problem. The PR AUC values are low, as is generally the case in eukaryotic GRN inference (Chen and Mar, 2018). Our comparison with several established gene expression-based GRN approaches, such as PANDA (Glass et al., 2013), ARACNE (Margolin et al., 2006), and corto (Mercatelli et al., 2020), shows that these methods also result in low PR AUC values. In addition to the improved performance, ANANSE has another clear benefit. While most GRN inference methods need a large collection of samples, ANANSE uses only two genome-wide measurements as input: gene expression and enhancer activity (H3K27ac ChIP-seq).

In contrast to previous approaches, our method takes advantage of TF binding in enhancers, instead of only gene expression

differences or TF binding to proximal promoters. This resulted in significantly improved performance, as benchmarked on experimentally validated trans-differentiation protocols. It has been previously shown that cell type-specific regulation is much better captured by enhancers as compared to promoter-proximal regulatory elements. For instance, TF binding and chromatin accessibility in distal elements better reflect the cell type identity of hematopoietic lineages than in promoters (Corces et al., 2016; Heinz et al., 2010). Many important transcriptional regulators mainly bind at regulatory regions that are not proximal to the promoter. Indeed, our analysis of the genomic binding distribution of ~300 human TFs showed that the large majority of cell type-specific TFs mainly binds in putative enhancer regions (Figure 1C). Therefore, we reasoned that TF binding at enhancers would be essential to model cell fate and lineage decisions. We tested the application of the networks inferred by ANANSE to human *in vitro* trans-differentiation approaches. Seminal work showed that computational algorithms can help to characterize cellular fate transitions, and to provide rational prioritization of TF candidates for trans-differentiation (Cahan et al., 2014; Morris et al., 2014; Rackham et al., 2016). We implemented a network-based approach to prioritize TFs that determine cell fate changes. Using a collection of known, experimentally validated trans-differentiation protocols, we demonstrated that ANANSE consistently outperforms other published approaches. This means that cellular trajectories can be characterized using ANANSE to identify the TFs that are involved in cell fate changes. In comparison with a promoter-based approach, we show that using enhancer-based regulatory information contributes significantly to this increased performance (Figure 5). One noticeable example is the trans-differentiation from fibroblasts or mesenchymal cells to keratinocytes. In current experimentally validated trans-differentiation methods, the epithelial master regulator TP63 is essential for establishing the keratinocyte cell fate (Chen et al., 2014; Kurita et al., 2018). However, TP63 was not predicted in most of the previously published computational methods (Cahan et al., 2014; Morris et al., 2014; Rackham et al., 2016). One plausible explanation is that TP63 is a TF for specific epithelial cells and tissues and it binds predominantly (87%) to enhancers (Andersson et al., 2014; Bulger and Groudine, 2011; Qu et al., 2018; Spitz and Furlong, 2012), whereas previous computational tools do not take enhancer properties into consideration.

We used ANANSE to identify tissue-specific TFs for different human tissues. We predicted the top 10 key TFs for all studied tissues. Many TFs in this list are known for important functions in these specific tissues. For example, some NK homeodomain, GATA, and T-box TFs are found in normal cardiac development, and have important functions during heart specification, patterning, and differentiation (Bruneau, 2013; Kathiriya et al., 2015; Stefanovic and Christoffels, 2015). Many SOX family of TFs are known critical regulators for neural system development in brain tissue (Bani-Yaghoub et al., 2006; Muto et al., 2009). Although not all predicted TFs are known to have important role in specific tissues, further research is warranted. The TFs in the TF atlas predicted by ANANSE may also be good candidates for studying tissue development and engineering in regenerative medicine

Another large benefit of the model that we implemented in ANANSE is the wide applicability. The source code is publicly available under a liberal license. It does not depend on large collections of reference data and it is straightforward to run on new data, such as different cell types or even species. The types of data required for this analysis are the following: gene expression data (RNA-seq) and a genome-wide measure of enhancer activity. The enhancer data consists of H3K27ac ChIP-seq, which is relatively easily obtained, not only in human cell types or in common model species, but also often in non-model species (Villar et al., 2015). The predictions of ANANSE (TF binding, gene regulatory networks and TFs ranked by influence) are useful to study gene regulatory principles in wide variety of contexts. While we used trans-differentiation experiments to benchmark the TF influence score, the utility of ANANSE is not limited to these types of experiments. It can also be used to study differentiation, cell type-specific gene regulation and developmental processes.

We also acknowledge limitations in our approach. In ANANSE, we link enhancer regions to genes on basis of distance. For each TF and gene interaction pair, ANANSE only considers TF binding information located at most 100kb up and downstream of the corresponding gene. Although data from a recent CRISPR enhancer interference screen showed that genomic distance is largely informative in predicting enhancer-target interactions (Fulco et al., 2019), this approach may be limited when applying to genes regulated through long-range regulation, especially those via inter-chromosomal regulation (Olivares-Chauvet et al., 2016). This limitation of our method can potentially be addressed using chromosome conformation capture techniques (3C) (Dekker et al., 2002) or other adaptations as circular 3C (4C) (Simonis et al., 2006; Zhao et al., 2006), chromosome conformation capture carbon copy (5C) (Dostie et al., 2006), chromatin immunoprecipitation using PET (ChIA-PET) (Fullwood et al., 2009) and Hi-C (Kempfer and Pombo, 2019). However, these types of data are currently only available for a limited number of cell types, therefore incorporation of topology data would limit the broad utility and application of our approach. Another limitation is that the current implementation of ANANSE focuses on activating transcription factors. During cell differentiation and reprogramming, other factors such as transcriptional repressors and chromatin modifying enzymes also play an important role. These are currently not considered in ANANSE. Finally, just like other genome-wide gene regulatory network inference methods, the performance of ANANSE is far from optimal. While our benchmarks (Figure 4 C and D, Supplemental Figure S3) indicate that the results of ANANSE are competitive with current methods based on correlation of gene expression, it is clear that there is still much progress to be made in genome-wide GRN inference.

Conclusion

Here we presented ANANSE, a computational tool for efficient predictions of TFs in cell fate determination. It outperforms other published methods in predicting TFs that can induce trans-differentiation. In addition, it is open source, freely available and can be easily used on custom data. In summary, ANANSE exploits the powerful impact enhancers have on gene regulatory networks, and it provides insights into TF mediated

regulatory mechanisms underlying cell fate determination and development.

Acknowledgements

We would like to thank the ENCODE DREAM challenge organizers for making consistently processed data available, and Jos Smits and Siebren Frölich for testing the ANANSE software package. We used the style from the Finkelstein lab at https://github.com/finkelsteinlab/BioRxiv-Template.

Notes

This article contains supporting information online.

Funding

QX was funded by the Chinese Scholarship Council (grant 201606230213). SJvH was supported by the Netherlands Organization for Scientific research (NWO grant 016.Vidi.189.081). Early work on this project was supported by a US National Institutes of Health grant (NICHD, R01HD069344) to GJCV.

Conflict of interest statement. None declared.

References

Andersson, R., Gebhard, C., Miguel-Escalada, I., Hoof, I., Bornholdt, J., Boyd, M., Chen, Y., Zhao, X., Schmidl, C., Suzuki, T., *et al.* (2014). An atlas of active enhancers across human cell types and tissues. Nature *507*, 455-461.

Bani-Yaghoub, M., Tremblay, R.G., Lei, J.X., Zhang, D., Zurakowski, B., Sandhu, J.K., Smith, B., Ribecco-Lutkiewicz, M., Kennedy, J., Walker, P.R., *et al.* (2006). Role of Sox2 in the development of the mouse neocortex. Dev Biol *295*, 52-66.

Batsis, J.A., Boateng, G.G., Seo, L.M., Petersen, C.L., Fortuna, K.L., Wechsler, E.V., Peterson, R.J., Cook, S.B., Pidgeon, D., Dokko, R.S., *et al.* (2019). Development and Usability Assessment of a Connected Resistance Exercise Band Application for Strength-Monitoring. World Acad Sci Eng Technol *13*, 340-348.

Bruneau, B.G. (2013). Signaling and transcriptional networks in heart development and regeneration. Cold Spring Harb Perspect Biol *5*, a008292.

Bruse, N., and Heeringen, S.J.v. (2018). GimmeMotifs: an analysis framework for transcription factor motif analysis. BioRxiv.

Budirahardja, Y., Tan, P.Y., Doan, T., Weisdepp, P., and Zaidel-Bar, R. (2016). The AP-2 Transcription Factor APTF-2 Is Required for Neuroblast and Epidermal Morphogenesis in Caenorhabditis elegans Embryogenesis. PLoS genetics *12*, e1006048.

Bulger, M., and Groudine, M. (2011). Functional and mechanistic diversity of distal transcription enhancers. Cell *144*, 327-339.

Buschbeck, M., and Hake, S.B. (2017). Variants of core histones and their roles in cell fate decisions, development and cancer. Nat Rev Mol Cell Biol *18*, 299-314.

Cahan, P., Li, H., Morris, S.A., Da Rocha, E.L., Daley, G.Q., and Collins, J.J. (2014). CellNet: network biology applied to stem cell engineering. Cell *158*, 903-915.

Caiazzo, M., Giannelli, S., Valente, P., Lignani, G., Carissimo, A., Sessa, A., Colasante, G., Bartolomeo, R., Massimino, L., and Ferroni, S. (2015). Direct conversion of fibroblasts into functional astrocytes by defined transcription factors. Stem cell reports *4*, 25-36.

Chen, S., and Mar, J.C. (2018). Evaluating methods of inferring gene regulatory networks highlights their lack of performance for single cell gene expression data. BMC Bioinformatics *19*, 232-232.

Chen, Y., Mistry, D.S., and Sen, G.L. (2014). Highly rapid and efficient conversion of human fibroblasts to keratinocyte-like cells. J Invest Dermatol *134*, 335-344.

Chèneby, J., Gheorghe, M., Artufel, M., Mathelier, A., and Ballester, B. (2017). ReMap 2018: an updated atlas of regulatory regions from an integrative analysis of DNA-binding ChIP-seq experiments. Nucleic acids research *46*, D267-D275.

Corces, M.R., Buenrostro, J.D., Wu, B., Greenside, P.G., Chan, S.M., Koenig, J.L., Snyder, M.P., Pritchard, J.K., Kundaje, A., Greenleaf, W.J., *et al.* (2016). Lineage-specific and single-cell chromatin accessibility charts human hematopoiesis and leukemia evolution. Nature genetics *48*, 1193-1203.

Cunningham, F., Achuthan, P., Akanni, W., Allen, J., Amode, M R., Armean, I.M., Bennett, R., Bhai, J., Billis, K., Boddu, S., *et al.* (2018). Ensembl 2019. Nucleic Acids Research *47*, D745-D751.

D'Alessio, A.C., Fan, Z.P., Wert, K.J., Baranov, P., Cohen, M.A., Saini, J.S., Cohick, E., Charniga, C., Dadon, D., and Hannett, N.M. (2015). A systematic approach to identify candidate transcription factors that control cell identity. Stem cell reports *5*, 763-775.

Daniely, Y., Liao, G., Dixon, D., Linnoila, R.I., Lori, A., Randell, S.H., Oren, M., and Jetten, A.M. (2004). Critical role of p63 in the development of a normal esophageal and tracheobronchial epithelium. Am J Physiol, Cell Physiol *287*, C171-C181.

Davidson, E.H. (2010). Emerging properties of animal gene regulatory networks. Nature *468*, 911-920.

Davis, C.A., Hitz, B.C., Sloan, C.A., Chan, E.T., Davidson, J.M., Gabdank, I., Hilton, J.A., Jain, K., Baymuradov, U.K., Narayanan, A.K., *et al.* (2018). The Encyclopedia of DNA elements (ENCODE): data portal update. Nucleic Acids Res *46*, D794-D801.

Davis, R.L., Weintraub, H., and Lassar, A.B. (1987). Expression of a single transfected cDNA converts fibroblasts to myoblasts. Cell *51*.

Dekker, J., Rippe, K., Dekker, M., and Kleckner, N. (2002). Capturing chromosome conformation. Science *295*, 1306-1311.

Dobin, A., Davis, C.A., Schlesinger, F., Drenkow, J., Zaleski, C., Jha, S., Batut, P., Chaisson, M., and Gingeras, T.R. (2013). STAR: ultrafast universal RNA-seq aligner. Bioinformatics *29*, 15-21.

Dollé, P.J.N.r.s. (2009). Developmental expression of retinoic acid receptors (RARs). Nuclear receptor signaling *7*, nrs. 07006.

Dostie, J., Richmond, T.A., Arnaout, R.A., Selzer, R.R., Lee, W.L., Honan, T.A., Rubio, E.D., Krumm, A., Lamb, J., Nusbaum, C.*, et al.* (2006). Chromosome Conformation Capture Carbon Copy (5C): a massively parallel solution for mapping interactions between genomic elements. Genome Res *16*, 1299-1309.

ENCODE Project Consortium (2012). An integrated encyclopedia of DNA elements in the human genome. Nature *489*, 57-74.

ENCODE-DREAM (2017). ENCODE-DREAM in vivo Transcription Factor Binding Site Prediction Challenge. Available from: https://www.synapse.org/ENCODE.

Feng, R., Desbordes, S.C., Xie, H., Tillo, E.S., Pixley, F., Stanley, E.R., and Graf, T. (2008). PU.1 and C/EBPα/β convert fibroblasts into macrophage-like cells. Proceedings of the National Academy of Sciences *105*, 6057-6062.

Fu, J.-D., Stone, N.R., Liu, L., Spencer, C.I., Qian, L., Hayashi, Y., Delgado-Olguin, P., Ding, S., Bruneau, B.G., and Srivastava, D. (2013). Direct reprogramming of human fibroblasts toward a cardiomyocyte-like state. Stem cell reports *1*, 235-247.

Fulco, C.P., Nasser, J., Jones, T.R., Munson, G., Bergman, D.T., Subramanian, V., Grossman, S.R., Anyoha, R., Patwardhan, T.A., Nguyen, T.H.*, et al.* (2019). Activity-by-Contact model of enhancer specificity from thousands of CRISPR perturbations. 529990.

Fullwood, M.J., Liu, M.H., Pan, Y.F., Liu, J., Xu, H., Mohamed, Y.B., Orlov, Y.L., Velkov, S., Ho, A., Mei, P.H.*, et al.* (2009). An oestrogen-receptor-alpha-bound human chromatin interactome. Nature *462*, 58-64.

Glass, K., Huttenhower, C., Quackenbush, J., and Yuan, G.-C. (2013). Passing Messages between Biological Networks to Refine Predicted Interactions. PLOS ONE *8*, e64832.

Han, H., Cho, J.-W., Lee, S., Yun, A., Kim, H., Bae, D., Yang, S., Kim, C.Y., Lee, M., and Kim, E. (2017). TRRUST v2: an expanded reference database of human and mouse transcriptional regulatory interactions. Nucleic acids research *46*, D380-D386.

Hartmann, A., Okawa, S., Zaffaroni, G., and Del Sol, A. (2018). SeesawPred: A Web Application for Predicting Cell-fate Determinants in Cell Differentiation. Sci Rep *8*, 13355.

Heinaniemi, M., Nykter, M., Kramer, R., Wienecke-Baldacchino, A., Sinkkonen, L., Zhou, J.X., Kreisberg, R., Kauffman, S.A., Huang, S., and Shmulevich, I. (2013). Gene-pair expression signatures reveal lineage control. Nat Methods *10*, 577-583.

Heinz, S., Benner, C., Spann, N., Bertolino, E., Lin, Y.C., Laslo, P., Cheng, J.X., Murre, C., Singh, H., and Glass, C.K. (2010). Simple combinations of lineage-determining transcription factors prime cis-regulatory elements required for macrophage and B cell identities. Molecular cell *38*, 576-589.

Hsu, F., Kent, W.J., Clawson, H., Kuhn, R.M., Diekhans, M., and Haussler, D. (2006). The UCSC known genes. Bioinformatics *22*, 1036-1046.

Huangfu, D., Osafune, K., Maehr, R., Guo, W., Eijkelenboom, A., Chen, S., Muhlestein, W., and Melton, D.A. (2008). Induction of pluripotent stem cells from primary human fibroblasts with only Oct4 and Sox2. Nat Biotechnol *26*, 1269-1275.

Ifkovits, J.L., Addis, R.C., Epstein, J.A., and Gearhart, J.D. (2014). Inhibition of TGFβ signaling increases direct conversion of fibroblasts to induced cardiomyocytes. PLoS One *9*, e89678.

Iwafuchi-Doi, M., and Zaret, K.S. (2016). Cell fate control by pioneer transcription factors. Development *143*, 1833-1837.

Jedlicka, P., Gutierrez-Hartmann, A.J.H., and histopathology (2008). Ets transcription factors in intestinal morphogenesis, homeostasis and disease. Histology and histopathology *23*, 1417.

Jopling, C., Boue, S., and Izpisua Belmonte, J.C. (2011). Dedifferentiation, transdifferentiation and reprogramming: three routes to regeneration. Nat Rev Mol Cell Biol *12*, 79-89.

Karimzadeh, M., and Hoffman, M.M. (2019). Virtual ChIP-seq: predicting transcription factor binding by learning from the transcriptome. bioRxiv, 168419.

Kathiriya, I.S., Nora, E.P., and Bruneau, B.G. (2015). Investigating the transcriptional control of cardiovascular development. Circulation research *116*, 700-714.

Katz, J.P., Perreault, N., Goldstein, B.G., Lee, C.S., Labosky, P.A., Yang, V.W., and Kaestner, K.H. (2002). The zinc-finger transcription factor Klf4 is required for terminal differentiation of goblet cells in the colon. Development *129*, 2619-2628.

Keilwagen, J., Posch, S., and Grau, J. (2019). Accurate prediction of cell type-specific transcription factor binding. Genome Biol *20*, 9.

Kempfer, R., and Pombo, A. (2019). Methods for mapping 3D chromosome architecture. Nat Rev Genet.

Kim, Y.J., Lim, H., Li, Z., Oh, Y., Kovlyagina, I., Choi, I.Y., Dong, X., and Lee, G. (2014). Generation of multipotent induced neural crest by direct reprogramming of human postnatal fibroblasts with a single transcription factor. Cell stem cell *15*, 497-506.

Kousa, Y.A., Fuller, E., and Schutte, B.C. (2018). IRF6 and AP2A Interaction Regulates Epidermal Development. The Journal of investigative dermatology *138*, 2578-2588.

Kurita, M., Araoka, T., Hishida, T., O'Keefe, D.D., Takahashi, Y., Sakamoto, A., Sakurai, M., Suzuki, K., Wu, J., and Yamamoto,

M. (2018). In vivo reprogramming of wound-resident cells generates skin epithelial tissue. Nature *561*, 243.

Lambert, S.A., Jolma, A., Campitelli, L.F., Das, P.K., Yin, Y., Albu, M., Chen, X., Taipale, J., Hughes, T.R., and Weirauch, M.T. (2018). The Human Transcription Factors. Cell *172*, 650-665.

Lang, A.H., Li, H., Collins, J.J., and Mehta, P. (2014). Epigenetic landscapes explain partially reprogrammed cells and identify key reprogramming genes. PLoS Comput Biol *10*, e1003734.

Li, H., Quang, D., and Guan, Y. (2019). Anchor: trans-cell type prediction of transcription factor binding sites. Genome Res *29*, 281-292.

Li, Q., Brown, J.B., Huang, H., and Bickel, P.J. (2011). Measuring reproducibility of high-throughput experiments. The annals of applied statistics *5*, 1752-1779.

Li, Y., Wang, Y., Yu, J., Ma, Z., Bai, Q., Wu, X., Bao, P., Li, L., Ma, D., and Liu, J. (2017). Direct conversion of human fibroblasts into osteoblasts and osteocytes with small molecules and a single factor, Runx2. bioRxiv, 127480.

Liberzon, A., Subramanian, A., Pinchback, R., Thorvaldsdóttir, H., Tamayo, P., and Mesirov, J.P. (2011). Molecular signatures database (MSigDB) 3.0. Bioinformatics *27*, 1739-1740.

Liu, Z.-P., Wu, C., Miao, H., and Wu, H. (2015). RegNetwork: an integrated database of transcriptional and post-transcriptional regulatory networks in human and mouse. Database *2015*.

Love, M.I., Huber, W., and Anders, S. (2014). Moderated estimation of fold change and dispersion for RNA-seq data with DESeq2. Genome Biology *15*, 550.

Luo, Z., Gao, X., Lin, C., Smith, E.R., Marshall, S.A., Swanson, S.K., Florens, L., Washburn, M.P., and Shilatifard, A. (2015). Zic2 is an enhancer-binding factor required for embryonic stem cell specification. Molecular cell *57*, 685-694.

Maag, J.L.V. (2018). gganatogram: An R package for modular visualisation of anatograms and tissues based on ggplot2. F1000Res *7*, 1576-1576.

Margolin, A.A., Nemenman, I., Basso, K., Wiggins, C., Stolovitzky, G., Dalla Favera, R., and Califano, A. (2006). ARACNE: an algorithm for the reconstruction of gene regulatory networks in a mammalian cellular context. BMC Bioinformatics *7 Suppl 1*, S7.

Meijer, D.H., Kane, M.F., Mehta, S., Liu, H., Harrington, E., Taylor, C.M., Stiles, C.D., and Rowitch, D.H. (2012). Separated at birth? The functional and molecular divergence of OLIG1 and OLIG2. Nat Rev Neurosci *13*, 819-831.

Mercatelli, D., Lopez-Garcia, G., and Giorgi, F.M. (2020). corto: a lightweight R package for gene network inference and master regulator analysis. Bioinformatics *36*, 3916-3917.

Morris, S.A., Cahan, P., Li, H., Zhao, A.M., San Roman, A.K., Shivdasani, R.A., Collins, J.J., and Daley, G.Q. (2014). Dissecting engineered cell types and enhancing cell fate conversion via CellNet. Cell *158*, 889-902.

Muto, A., Iida, A., Satoh, S., and Watanabe, S. (2009). The group E Sox genes Sox8 and Sox9 are regulated by Notch signaling and are required for Muller glial cell development in mouse retina. Exp Eye Res *89*, 549-558.

Nair, M., Teng, A., Bilanchone, V., Agrawal, A., Li, B., and Dai, X. (2006). Ovol1 regulates the growth arrest of embryonic epidermal progenitor cells and represses c-myc transcription. J Cell Biol *173*, 253-264.

Nakamori, D., Akamine, H., Takayama, K., Sakurai, F., and Mizuguchi, H. (2017). Direct conversion of human fibroblasts into hepatocyte-like cells by ATF5, PROX1, FOXA2, FOXA3, and HNF4A transduction. Sci Rep *7*, 16675.

Novakovic, B., Habibi, E., Wang, S.-Y., Arts, R.J., Davar, R., Megchelenbrink, W., Kim, B., Kuznetsova, T., Kox, M., and Zwaag, J. (2016). β-Glucan reverses the epigenetic state of LPS-induced immunological tolerance. Cell *167*, 1354-1368. e1314.

Obayashi, T., Kagaya, Y., Aoki, Y., Tadaka, S., and Kinoshita, K. (2019). COXPRESdb v7: a gene coexpression database for 11 animal species supported by 23 coexpression platforms for technical evaluation and evolutionary inference. Nucleic Acids Res *47*, D55-D62.

Oberbeck, N., Pham, V.C., Webster, J.D., Reja, R., Huang, C.S., Zhang, Y., Roose-Girma, M., Warming, S., Li, Q., Birnberg, A.*, et al.* (2019). The RIPK4-IRF6 signalling axis safeguards epidermal differentiation and barrier function. Nature *574*, 249-253.

Ohteki, T., Maki, C., and Koyasu, S. (2001). Overexpression of Bcl-2 Differentially Restores Development of Thymus-Derived CD4[−]8⁺ T Cells and Intestinal Intraepithelial T Cells in IFN-Regulatory Factor-1-Deficient Mice. *166*, 6509-6513.

Olivares-Chauvet, P., Mukamel, Z., Lifshitz, A., Schwartzman, O., Elkayam, N.O., Lubling, Y., Deikus, G., Sebra, R.P., and Tanay, A. (2016). Capturing pairwise and multi-way chromosomal conformations using chromosomal walks. Nature *540*, 296-300.

Pang, Z.P., Yang, N., Vierbuchen, T., Ostermeier, A., Fuentes, D.R., Yang, T.Q., Citri, A., Sebastiano, V., Marro, S., Südhof, T.C.*, et al.* (2011). Induction of human neuronal cells by defined transcription factors. Nature *476*, 220-223.

Patro, R., Duggal, G., Love, M.I., Irizarry, R.A., and Kingsford, C. (2017). Salmon provides fast and bias-aware quantification of transcript expression. Nature methods *14*, 417-419.

Pedregosa, F., Varoquaux, G., Gramfort, A., Michel, V., Thirion, B., Grisel, O., Blondel, M., Prettenhofer, P., Weiss, R., and Dubourg, V. (2011). Scikit-learn: Machine learning in Python. the Journal of machine Learning research *12*, 2825-2830.

Peñalosa-Ruiz, G., Bright, A.R., Mulder, K.W., and Veenstra, G.J.C. (2019). The interplay of chromatin and transcription factors during cell fate transitions in development and reprogramming. Biochim Biophys Acta Gene Regul Mech *1862*, 194407.

Picard2019toolkit (2019). Picard toolkit. Broad Institute, GitHub repository.

Qin, Q., Fan, J., Zheng, R., Wan, C., Mei, S., Wu, Q., Sun, H., Brown, M., Zhang, J., Meyer, C.A.*, et al.* (2020). Lisa: inferring transcriptional regulators through integrative modeling of public chromatin accessibility and ChIP-seq data. Genome Biol *21*, 32.

Qu, J., Tanis, S.E., Smits, J.P., Kouwenhoven, E.N., Oti, M., van den Bogaard, E.H., Logie, C., Stunnenberg, H.G., van Bokhoven, H., and Mulder, K.W. (2018). Mutant p63 affects epidermal cell identity through rewiring the enhancer landscape. Cell reports *25*, 3490-3503. e3494.

Quang, D., and Xie, X. (2019). FactorNet: A deep learning framework for predicting cell type specific transcription factor binding from nucleotide-resolution sequential data. Methods *166*, 40-47.

Quinlan, A.R., and Hall, I.M. (2010). BEDTools: a flexible suite of utilities for comparing genomic features. Bioinformatics *26*, 841-842.

Rackham, O.J., Firas, J., Fang, H., Oates, M.E., Holmes, M.L., Knaupp, A.S., Suzuki, H., Nefzger, C.M., Daub, C.O., and Shin, J.W. (2016). A predictive computational framework for direct reprogramming between human cell types. Nature genetics *48*, 331.

Reik, W., Dean, W., and Walter, J. (2001). Epigenetic reprogramming in mammalian development. Science (New York, NY) *293*, 1089-1093.

Richardson, R.J., Dixon, J., Malhotra, S., Hardman, M.J., Knowles, L., Boot-Handford, R.P., Shore, P., Whitmarsh, A., and Dixon, M.J. (2006). Irf6 is a key determinant of the keratinocyte proliferation-differentiation switch. Nature genetics *38*, 1329-1334.

Roost, M.S., van Iperen, L., Ariyurek, Y., Buermans, H.P., Arindrarto, W., Devalla, H.D., Passier, R., Mummery, C.L., Carlotti, F., de Koning, E.J.*, et al.* (2015). KeyGenes, a Tool to Probe Tissue Differentiation Using a Human Fetal Transcriptional Atlas. Stem Cell Reports *4*, 1112-1124.

Ruberte, E., Dolle, P., Krust, A., Zelent, A., Morriss-Kay, G., and Chambon, P. (1990). Specific spatial and temporal distribution of retinoic acid receptor gamma transcripts during mouse embryogenesis. *108*, 213-222.

Saito, T., and Rehmsmeier, M. (2015). The precision-recall plot is more informative than the ROC plot when evaluating binary classifiers on imbalanced datasets. PLoS One *10*, e0118432.

Sen, G.L., Boxer, L.D., Webster, D.E., Bussat, R.T., Qu, K., Zarnegar, B.J., Johnston, D., Siprashvili, Z., and Khavari, P.A. (2012). ZNF750 is a p63 target gene that induces KLF4 to drive terminal epidermal differentiation. Dev Cell *22*, 669-677.

Sergushichev, A. (2016). An algorithm for fast preranked gene set enrichment analysis using cumulative statistic calculation. BioRxiv, 060012.

Simeonov, K.P., and Uppal, H. (2014). Direct reprogramming of human fibroblasts to hepatocyte-like cells by synthetic modified mRNAs. PloS one *9*, e100134.

Simonis, M., Klous, P., Splinter, E., Moshkin, Y., Willemsen, R., de Wit, E., van Steensel, B., and de Laat, W. (2006). Nuclear organization of active and inactive chromatin domains uncovered by chromosome conformation capture-on-chip (4C). Nat Genet *38*, 1348-1354.

Soares, E., Xu, Q., Li, Q., Qu, J., Zheng, Y., Raeven, H.H., Brandao, K.O., Petit, I., van den Akker, W.M., and van Heeringen, S.J. (2019). Single-cell RNA-seq identifies a reversible mesodermal activation in abnormally specified epithelia of p63 EEC syndrome. Proceedings of the National Academy of Sciences *116*, 17361-17370.

Soneson, C., Love, M.I., and Robinson, M.D. (2015). Differential analyses for RNA-seq: transcript-level estimates improve gene-level inferences. F1000Res *4*, 1521.

Spitz, F., and Furlong, E.E.M. (2012). Transcription factors: from enhancer binding to developmental control. Nat Rev Genet *13*, 613-626.

Stadhouders, R., Filion, G.J., and Graf, T. (2019). Transcription factors and 3D genome conformation in cell-fate decisions. Nature *569*, 345-354.

Stefanovic, S., and Christoffels, V.M. (2015). GATA-dependent transcriptional and epigenetic control of cardiac lineage specification and differentiation. Cell Mol Life Sci *72*, 3871-3881.

Takahashi, K., Tanabe, K., Ohnuki, M., Narita, M., Ichisaka, T., Tomoda, K., and Yamanaka, S. (2007). Induction of pluripotent stem cells from adult human fibroblasts by defined factors. Cell *131*, 861-872.

Tchieu, J., Calder, E.L., Guttikonda, S.R., Gutzwiller, E.M., Aromolaran, K.A., Steinbeck, J.A., Goldstein, P.A., and Studer, L. (2019). NFIA is a gliogenic switch enabling rapid derivation of functional human astrocytes from pluripotent stem cells. Nature biotechnology *37*, 267.

Tegner, J., and Bjorkegren, J. (2007). Perturbations to uncover gene networks. Trends Genet *23*, 34-41.

The Gene Ontology, C. (2019). The Gene Ontology Resource: 20 years and still GOing strong. Nucleic Acids Res *47*, D330-D338.

Thompson, C.A., DeLaForest, A., and Battle, M.A. (2018). Patterning the gastrointestinal epithelium to confer regional-specific functions. Dev Biol *435*, 97-108.

Tsuji, G., Ito, T., Chiba, T., Mitoma, C., Nakahara, T., Uchi, H., and Furue, M. (2018). The role of the OVOL1-OVOL2 axis in normal and diseased human skin. J Dermatol Sci *90*, 227-231.

Uhlén, M., Fagerberg, L., Hallström, B.M., Lindskog, C., Oksvold, P., Mardinoglu, A., Sivertsson, Å., Kampf, C., Sjöstedt, E., and

Asplund, A. (2015). Tissue-based map of the human proteome. Science *347*, 1260419.

Uhlen, M., Oksvold, P., Fagerberg, L., Lundberg, E., Jonasson, K., Forsberg, M., Zwahlen, M., Kampf, C., Wester, K., and Hober, S. (2010). Towards a knowledge-based human protein atlas. Nature biotechnology *28*, 1248.

Valouev, A., Johnson, D.S., Sundquist, A., Medina, C., Anton, E., Batzoglou, S., Myers, R.M., and Sidow, A. (2008). Genome-wide analysis of transcription factor binding sites based on ChIP-Seq data. Nature methods *5*, 829.

van der Raadt, J., van Gestel, S.H., Nadif Kasri, N., and Albers, C.A. (2019). ONECUT transcription factors induce neuronal characteristics and remodel chromatin accessibility. Nucleic acids research *47*, 5587-5602.

van Heeringen, S.J., and Veenstra, G.J.C. (2010). GimmeMotifs: a de novo motif prediction pipeline for ChIP-sequencing experiments. Bioinformatics *27*, 270-271.

Vaquerizas, J.M., Kummerfeld, S.K., Teichmann, S.A., and Luscombe, N.M. (2009). A census of human transcription factors: function, expression and evolution. Nat Rev Genet *10*, 252-263.

Vierbuchen, T., Ostermeier, A., Pang, Z.P., Kokubu, Y., Südhof, T.C., and Wernig, M. (2010). Direct conversion of fibroblasts to functional neurons by defined factors. Nature *463*, 1035-1041.

Villar, D., Berthelot, C., Aldridge, S., Rayner, T.F., Lukk, M., Pignatelli, M., Park, T.J., Deaville, R., Erichsen, J.T., Jasinska, A.J.*, et al.* (2015). Enhancer evolution across 20 mammalian species. Cell *160*, 554-566.

Wang, S., Zang, C., Xiao, T., Fan, J., Mei, S., Qin, Q., Wu, Q., Li, X., Xu, K., and He, H.H. (2016). Modeling cis-regulation with a compendium of genome-wide histone H3K27ac profiles. Genome research *26*, 1417-1429.

Wang, X., Pasolli, H.A., Williams, T., and Fuchs, E. (2008). AP-2 factors act in concert with Notch to orchestrate terminal differentiation in skin epidermis. J Cell Biol *183*, 37-48.

Weirauch, M.T., Yang, A., Albu, M., Cote, A.G., Montenegro-Montero, A., Drewe, P., Najafabadi, H.S., Lambert, S.A., Mann, I., and Cook, K. (2014). Determination and inference of eukaryotic transcription factor sequence specificity. Cell *158*, 1431-1443.

Wilanowski, T., Caddy, J., Ting, S.B., Hislop, N.R., Cerruti, L., Auden, A., Zhao, L.L., Asquith, S., Ellis, S., Sinclair, R.*, et al.* (2008). Perturbed desmosomal cadherin expression in grainy head-like 1-null mice. EMBO J *27*, 886-897.

Wilkinson, A.C., Nakauchi, H., and Göttgens, B. (2017). Mammalian Transcription Factor Networks: Recent Advances in Interrogating Biological Complexity. Cell Syst *5*, 319-331.

Xie, H., Ye, M., Feng, R., and Graf, T. (2004). Stepwise reprogramming of B cells into macrophages. Cell *117*, 663-676.

Xiong, Z., Ren, S., Chen, H., Liu, Y., Huang, C., Zhang, Y.L., Odera, J.O., Chen, T., Kist, R., Peters, H.*, et al.* (2018). PAX9 regulates squamous cell differentiation and carcinogenesis in the oro-oesophageal epithelium. J Pathol *244*, 164-175.

Yamamoto, K., Kishida, T., Sato, Y., Nishioka, K., Ejima, A., Fujiwara, H., Kubo, T., Yamamoto, T., Kanamura, N., and Mazda, O. (2015). Direct conversion of human fibroblasts into functional osteoblasts by defined factors. Proc Natl Acad Sci U S A *112*, 6152-6157.

Yu, G., Wang, L.-G., and He, Q.-Y. (2015). ChIPseeker: an R/Bioconductor package for ChIP peak annotation, comparison and visualization. Bioinformatics (Oxford, England) *31*, 2382-2383.

Yu, J., Vodyanik, M.A., Smuga-Otto, K., Antosiewicz-Bourget, J., Frane, J.L., Tian, S., Nie, J., Jonsdottir, G.A., Ruotti, V., Stewart, R.*, et al.* (2007). Induced pluripotent stem cell lines derived from human somatic cells. Science *318*, 1917-1920.

Zhang, Y., Liu, T., Meyer, C.A., Eeckhoute, J., Johnson, D.S., Bernstein, B.E., Nusbaum, C., Myers, R.M., Brown, M., and Li, W. (2008). Model-based analysis of ChIP-Seq (MACS). Genome biology *9*, R137.

Zhao, Z., Tavoosidana, G., Sjölinder, M., Göndör, A., Mariano, P., Wang, S., Kanduri, C., Lezcano, M., Sandhu, K.S., Singh, U.*, et al.* (2006). Circular chromosome conformation capture (4C) uncovers extensive networks of epigenetically regulated intra- and interchromosomal interactions. Nat Genet *38*, 1341-1347.

Supplementary information

Additional file 1:
Figure S1. ROC curve analysis of TF binding prediction performance.
Figure S2. ROC curve analysis of TF binding prediction performance.
Figure S3. Evaluation of cell type-specific enhancer gene regulatory networks.
Figure S4. Comparison of the top 10 key TFs predicted by different GRN sizes in seven experimentally validated trans-differentiation strategies.
Figure S5. Comparison of different GRN sizes used in the ANANSE prediction in seven experimentally validated trans-differentiation strategies.
Figure S6. Comparison of the top 10 key TFs predicted by different GRNs (enhancer, promoter and expression) in seven experimentally validated trans-differentiation strategies.
Figure S7. Comparison of the top 10 key TFs predicted by different methods in seven experimentally validated trans-differentiation strategies.
Figure S8. Classification of the human gene expression and TF influence score.

Additional file 2: Table S1. Trans-differentiation expression dataset

Additional file 3: Table S2. Trans-differentiation differentially expressed gene dataset

Additional file 4: Table S3. Trans-differentiation enhancer dataset

Additional file 5: Table S4. TF binding sites genomic location summary

Additional file 6: Table S5. TF binding site prediction validation results

Additional file 9: Table S6. Trans-differentiation key TFs prediction results among enhancer promoter and expression network

Additional file 10: Table S7. Application of ANANSE to human tissues data results

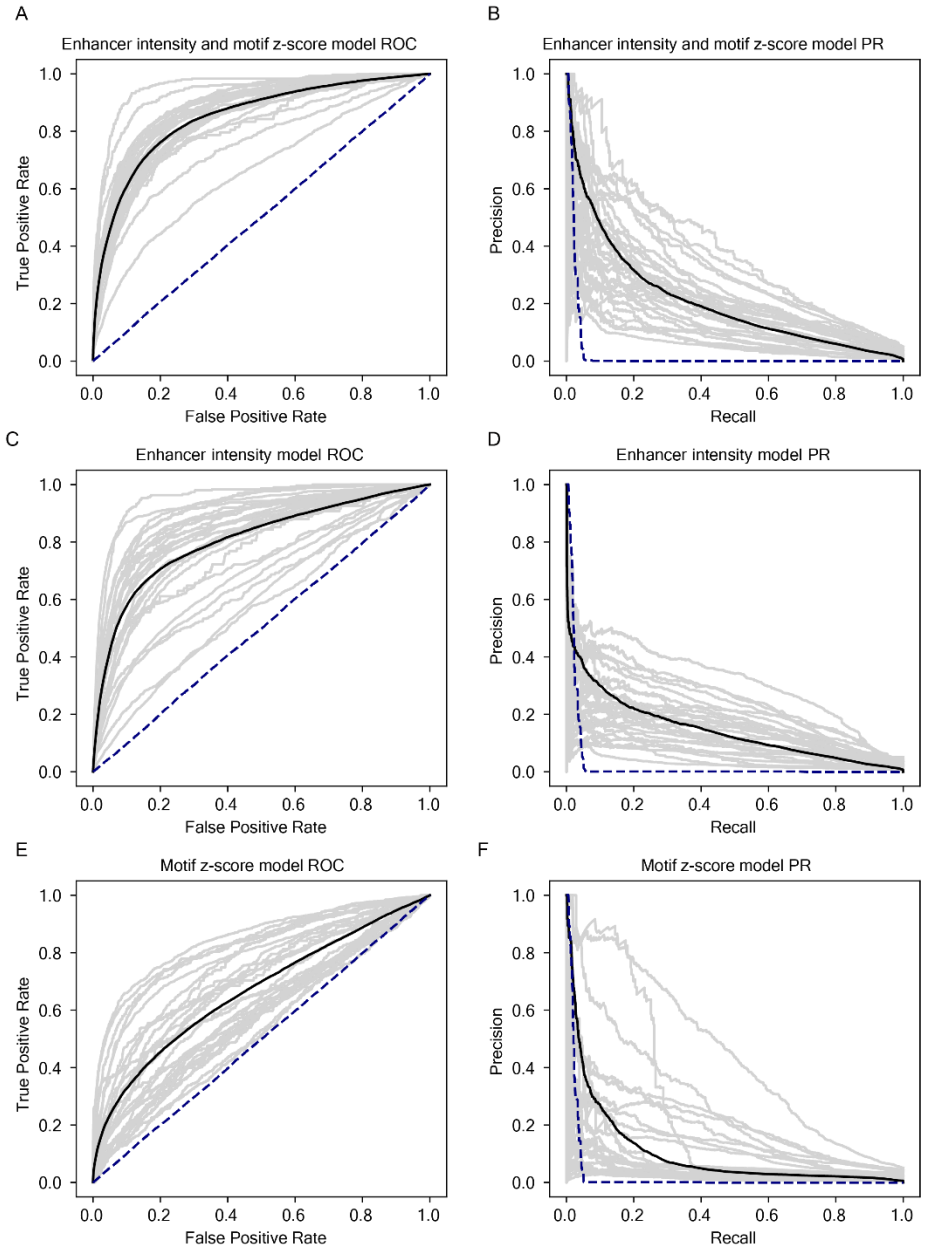

Supplementary Figure S1. ROC curve analysis of TF binding prediction performance.
(A) ROC curves of TF binding prediction based on enhancer intensities together with motif z-scores. Each line represents one TF prediction result based on the model trained on data from all the other 27 TFs. **(B)** PR curves of TF binding prediction based on enhancer intensities together with motif z-scores. **(C)** ROC curves of TF binding prediction based on enhancer intensities. **(D)** PR curves of TF binding based on enhancer intensities **(E)** ROC curves of TF binding prediction based on motif z-scores. **(F)** PR curves of TF binding prediction based on motif z-scores.

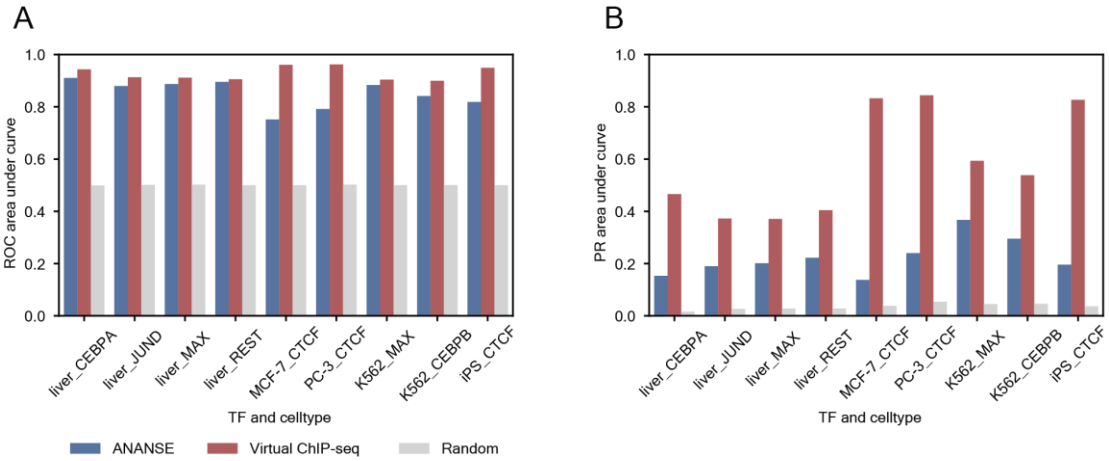

Supplementary Figure S2. ROC and PR curve analysis of TF binding prediction performance. **(A)** The barplot shows ROC AUC of TF binding prediction of ANANSE compared to the Virtual ChIP-seq predictions in the ENCODE-DREAM validation cell types. ROC AUC of the ANANSE predicted TF binding is shown in blue; the Virtual ChIP-seq predicted result in red and the random model is indicated in gray. **(B)** The same evaluation as in A), with the PR AUC shown as a barplot.

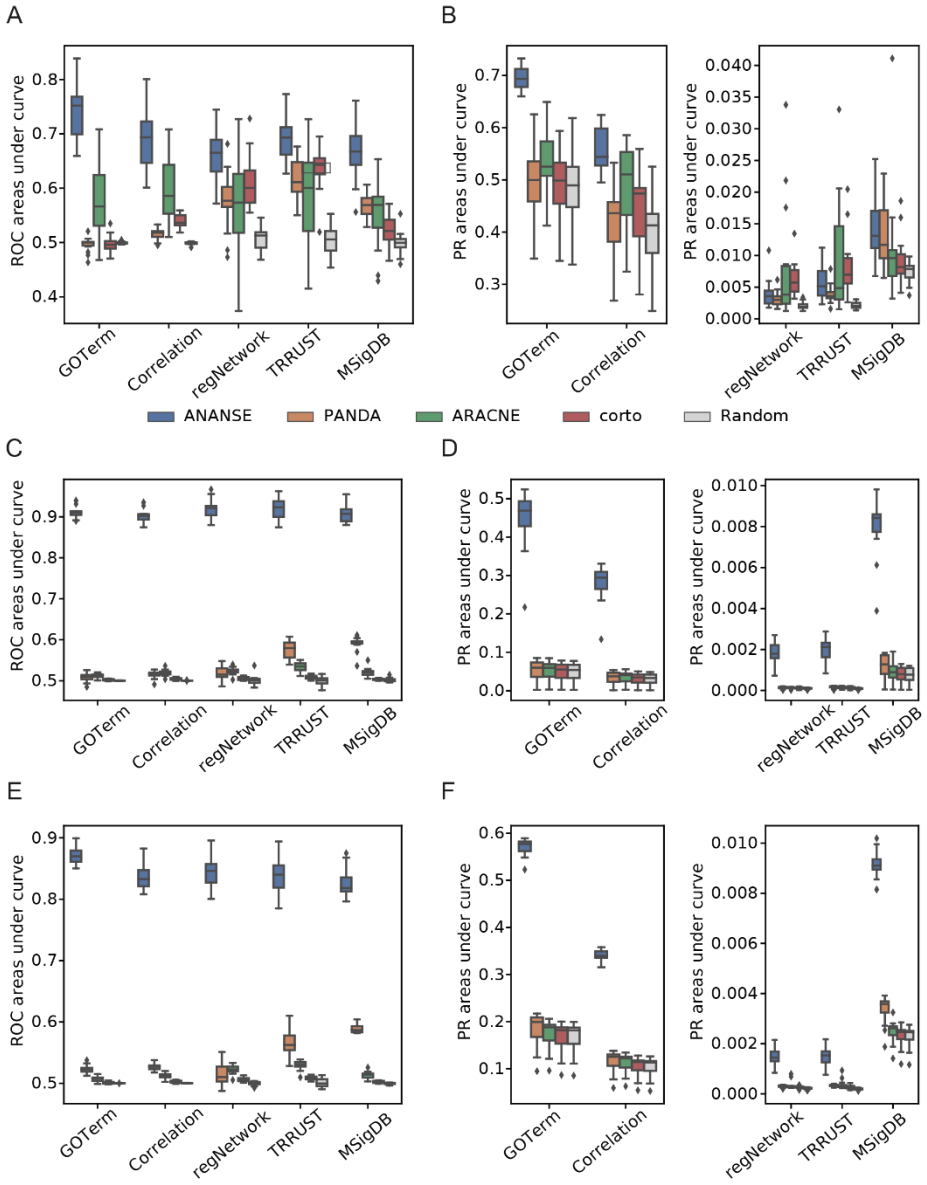

Supplementary Figure S3. Evaluation of cell type-specific enhancer gene regulatory networks. **(A)** Evaluation of the predicted networks using different types of data: a gene ontology (GO) term co-regulatory network, a cell type-specific gene correlation network, and three TF-Gene regulatory networks based on interaction databases (regNetwork, TRRUST, and MSigDB C3). This is the same evaluation as presented in Figure 4C-D, but using a TPM cutoff of 1 instead of 10 and the intersection of the network edges among the four predicted GRNs. The boxplots show the AUC of the ROC for 15 different tissues. ROC AUC of the ANANSE predicted networks is shown in blue; the PANDA networks in orange; the ARACNE networks in green; the corto networks in red; the random networks are indicated in gray. **(B)** The same evaluation as in A), with the PR AUC shown as a boxplot. **(C)** The same evaluation as in Figure 4C-D, with a TPM cutoff of 10 and the union of all network edges among the four predicted GRNs as reference interactions. **(D)** The same evaluation as in C), with the PR AUC shown as a boxplot. **(E)** The same evaluation as in A), with a TPM cutoff of 10 and the union of all network edges among four predicted GRNs as reference interactions. **(F)** The same evaluation as in E), with the PR AUC shown as a boxplot.

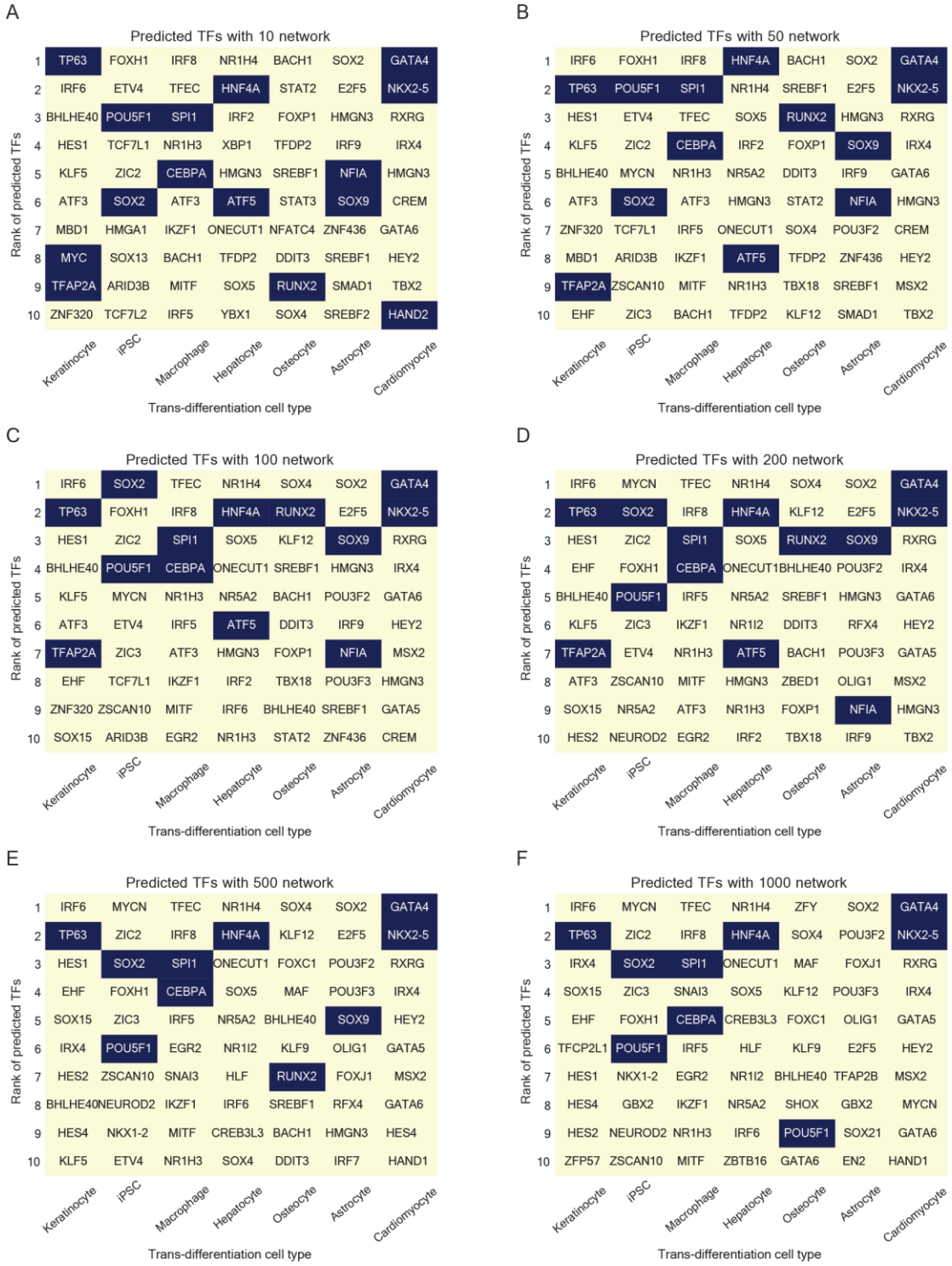

Supplementary Figure S4. Comparison of the top 10 key TFs predicted by different GRN sizes in seven experimentally validated trans-differentiation strategies.

The x-axis shows seven experimentally validated trans-differentiations, and the y-axis shows the top 10 predicted key TFs ranked by their influence score. Black boxes highlight the TFs that were used in trans-differentiation experiments. **(A)** 10k network. **(B)** 50k network. **(C)** 100k network. **(D)** 200k network. **(E)** 500k network. **(F)** 1000k network.

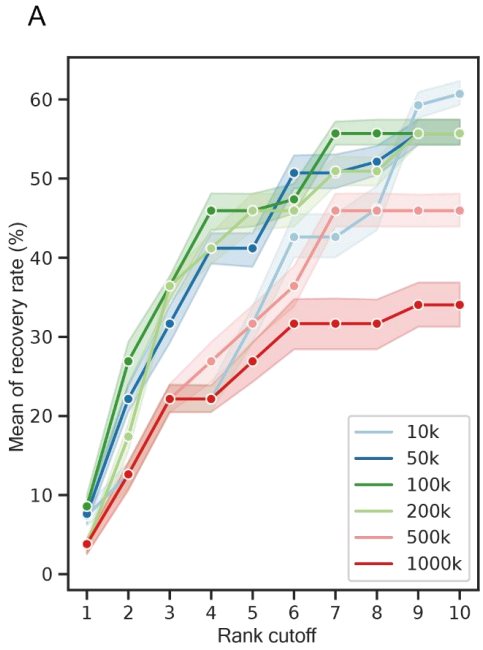

Supplementary Figure S5. Comparison of different GRN sizes used in the ANANSE prediction in seven experimentally validated trans-differentiation strategies.
(A) The line plots show the comparison of the predicted key TFs for six different sizes of GRNs Shown is the fraction of predicted TFs compared to all known TFs based on trans-differentiation protocols described in the literature (y-axis) as a function of the top number of TFs selected (x-axis). The shaded area represents the minimum and maximum percentage of corresponding recovered TFs when using six out of seven trans-differentiations.

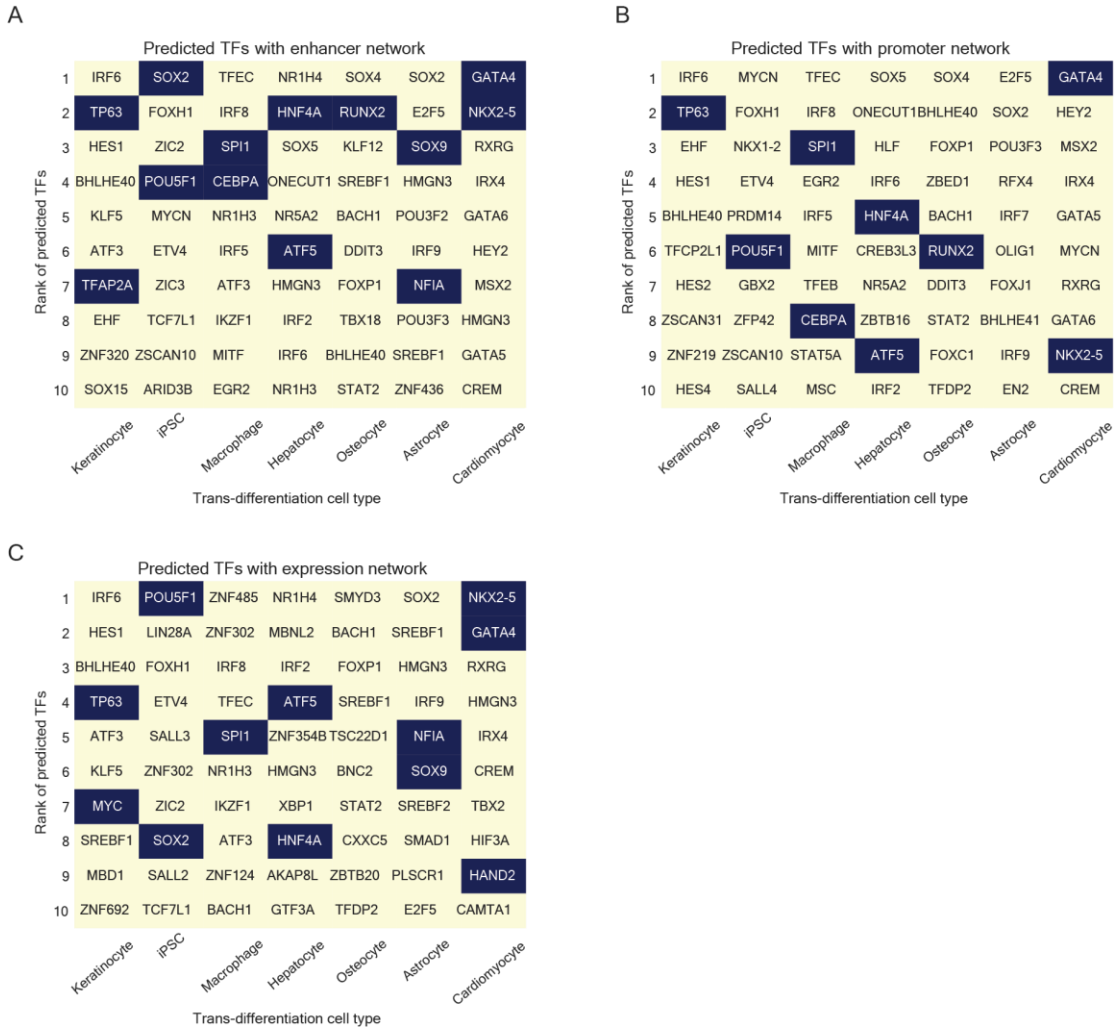

Supplementary Figure S6. Comparison of the top 10 key TFs predicted by different GRNs (enhancer, promoter and expression) in seven experimentally validated trans-differentiation strategies.

The x-axis shows seven experimentally validated trans-differentiations, and the y-axis shows the top 10 predicted key TFs ranked by their influence score. Black boxes highlight the TFs that were used in trans-differentiation experiments. **(A)** The results for ANANSE, based on a GRN that was inferred using peaks, regardless of their genomic location (includes both promoters and enhancers). **(B)** The results for ANANSE, based on a GRN that was inferred using the highest peak in the gene promoter, defined as < 2kb from the gene transcription start site. **(C)** The results for ANANSE, based on a GRN that was inferred using only the expression levels of the TFs and target genes.

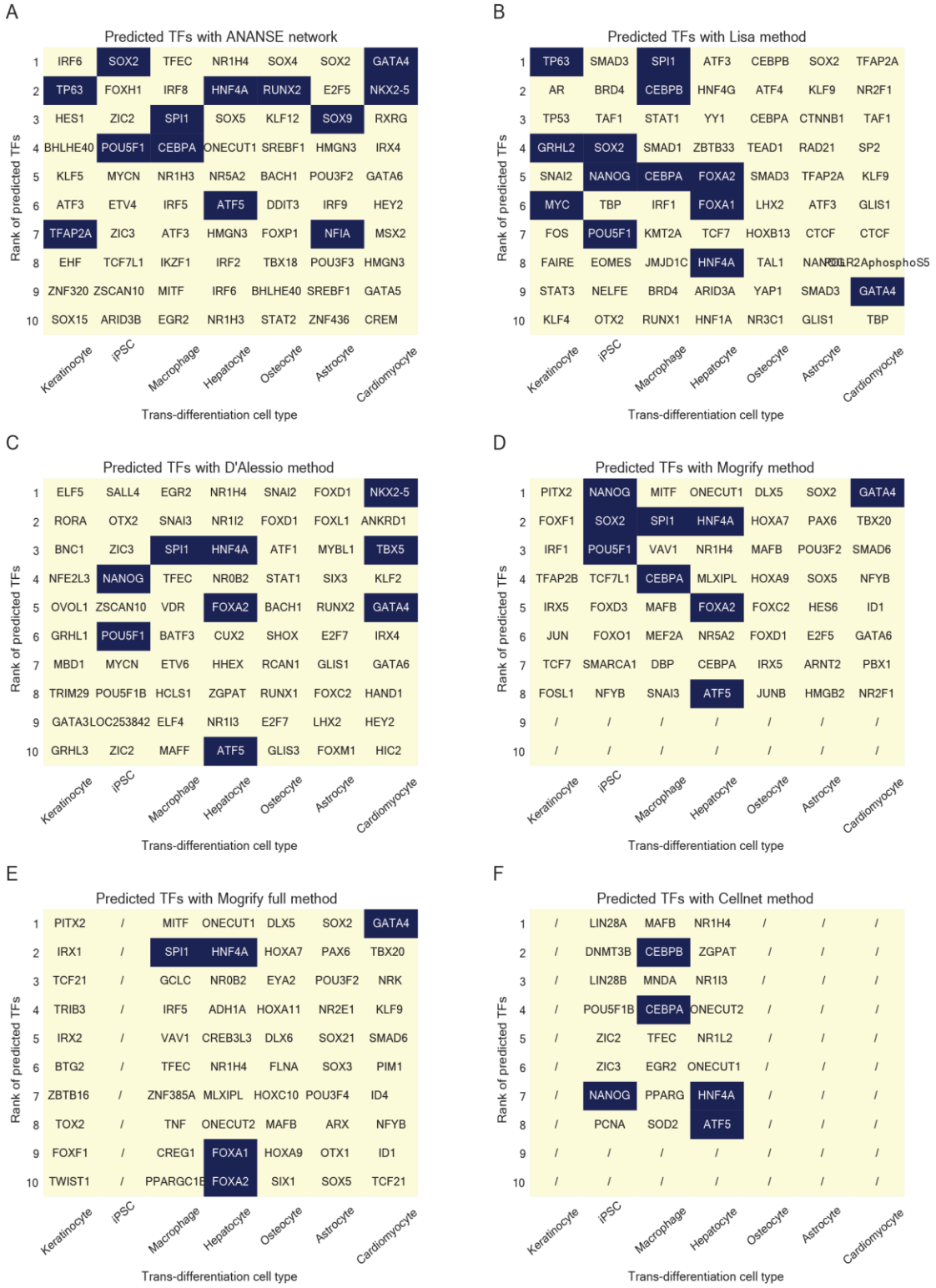

Supplementary Figure S7. Comparison of the top 10 key TFs predicted by different methods in seven experimentally validated trans-differentiation strategies.

The x-axis shows seven experimentally validated trans-differentiations, and the y-axis shows the top 10 predicted key TFs ranked by their influence score. Black boxes highlight the TFs that were used in trans-differentiation experiments. **(A)** ANANSE. **(B)** Lisa. **(C)** D'Alessio. **(D)** Mogrify. **(E)** Mogrify full list. **(F)** CellNet.

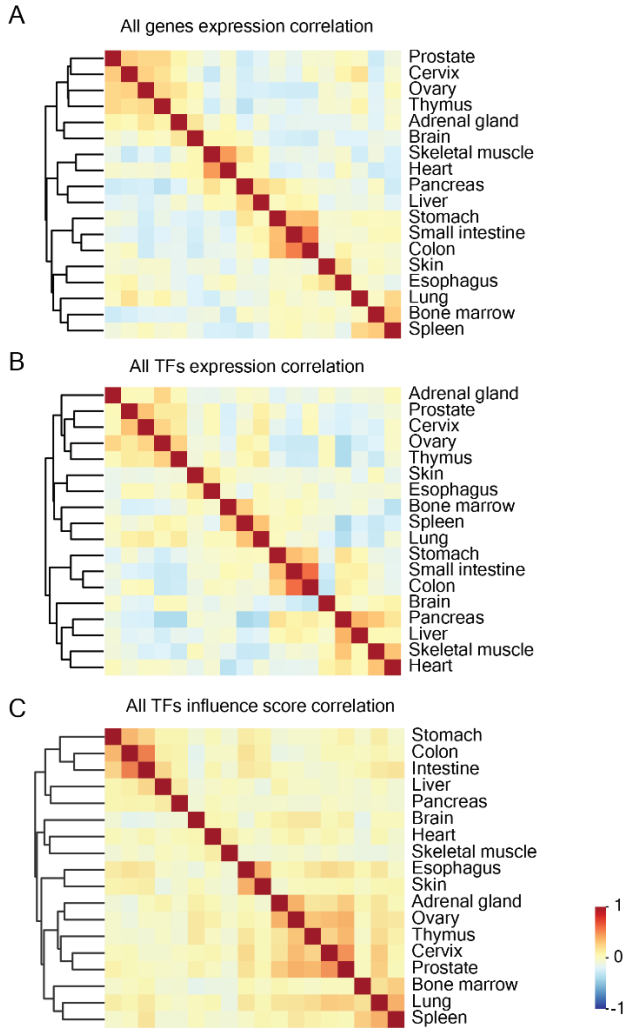

Supplementary Figure S8. Classification of the human gene expression and TF influence score. **(A)**, Heatmap showing the pairwise correlation between all 18 tissues based on gene expression. The colors in the heatmap indicate high (red) or low (blue) correlation across the tissue set. **(B)**, Heatmap showing the pairwise correlation between all 18 tissues based on the expression of all TFs. **(C)**, Heatmap showing the pairwise correlation between all 18 tissues based on TF influence scores.